Investigation of Diffusion in Spark Plasma Sintering through the Copper-Nickel System

Samantha Rudinsky

Department of Mining and
Materials Engineering

McGill University
Montreal

August 2014

A thesis submitted to McGill University in partial fulfillment of the requirements of the degree of Masters of Engineering

Abstract

The effect of current on diffusion in spark plasma sintering (SPS) was investigated using the Cu-Ni system. The 1D case was first investigated through the use of binary diffusion couples generated from bulk material. Subsequently, diffusion was studied in 3D by sintering a blend of nickel and copper powders.

Copper and nickel diffusion couples were generated in SPS and in a horizontal insertion vacuum furnace. In SPS, two separate orientations were processed: one where copper diffusion occurred in the same direction as the current, denoted Cu/Ni, and another where current passed in the opposite direction of the diffusing copper, denoted Ni/Cu. Experiments were performed at temperatures between 750^{o}C and 1000^{o}C for 1h, 2h, and 3h. Line scans were obtained by energy-dispersive spectroscopy (EDS) and corresponding weight fractions of copper were calculated to obtain concentration profiles. Diffusion coefficients were calculated using the Sauer-Freise den Broeder (SFB) method and corresponding activation energies were obtained. It was found that, while at lower temperatures all concentration profiles were similar, at temperatures of 950^{o}C and 1000^{o}C, the diffusion distance of the SPS samples was reduced compared to those annealed without current. Consequently, diffusion coefficients of these samples were also lower. Activation energy for diffusion was reduced in SPS compared to annealing without current. It was deduced that the reduction in diffusion was a result of the application of current coupled with the loss in ferromagnetism of nickel. Clustering of nickel atoms occurs at high temperatures due to the following, a re-arrangement of electrons in the nickel band structure and an increase of electrons in the conduction band arising from the application of current. This causes a repulsive chemical potential between the copper atoms and the nickel clusters. The decrease in activation energy is the result of temperature gradients existing within the diffusion couple. These gradients are caused by the difference in resistivity between the two species.

To study diffusion in 3D, a powder blend of spherical copper and nickel powders was produced in order to obtain a mix containing 5 wt% Cu. Pucks of this blend were sintered at 700, 800, and

900^{o}C for 30 minutes. Isolated copper particles were found using backscattered electron (BSE) imaging and EDS maps were obtained of the particle and its surrounding areas. It was found that copper diffuses throughout the nickel matrix uniformly with no higher diffusing paths in any specific direction. Diffusion coefficients and activation energies were calculated and it was shown that diffusion occurs similarly perpendicular and parallel to the applied current. Given the infinite binary diffusion couple model solution and the homogenization model solution to the non-steady state diffusion equation, it was determined that the amount of time required to obtain a final product with a homogeneous distribution of copper in SPS surpasses typical sintering times used in conventional methods.

Résumé

L'effet du courant sur la diffusion par frittage à chaud avec champ électrique pulsé (SPS) a été investigué en utilisant le system Cu-Ni. En premier, le cas en 1D a été étudié à travers l'utilisation de couples de diffusion binaires produites de matériel en vrac. Par après, la diffusion a été étudiée en 3D en frittant un mélange de poudres de cuivre et nickel.

Des couples de diffusion de cuivre et nickel ont été générés dans l'SPS et dans une fournaise d'insertion horizontale. En SPS, deux orientations différentes ont été fabriquées : une où la diffusion du cuivre se faisait dans la même direction que le courant, notée Cu/Ni, et l'autre où le courant passait dans la direction inverse du cuivre diffusé, notée Ni/Cu. Des expériences ont été effectuées à des températures entre 750 et 1000^{o}C pour 1, 2 et 3h. Des scans linéaires ont été obtenu par analyse dispersive en énergie (EDS) et les fractions de poids correspondantes ont été calculés pour obtenir des profiles de concentration. Les coefficients de diffusion ont été calculés par la méthode Sauer-Freise den Broeder (SFB) et les énergies d'activation ont été obtenues pour ces valeurs. C'était trouvé que, quand aux basses températures, toutes les profiles de concentrations étaient similaires, mais, vers 950^{o}C et 1000^{o}C, la distance de diffusion en SPS était réduite comparer à ceux chauffés sans courant. Par conséquence, les coefficients de diffusion pour les échantillons produits par SPS étaient baissés aussi. L'énergie d'activation était réduite en SPS comparer à ceux chauffés sans courant. C'était déduit que la réduction de diffusion était le résultat de l'application de courant couplée avec la perte de ferromagnétisme du nickel. Des regroupements d'atomes de nickel se produisent à des températures élevées dû aux phénomènes suivants, les électrons dans la structure de band du nickel se réarrangent et il y a un surplus d'électrons dans la bande conductrice qui se réorientent aussi. Ceci cause un potentiel chimique répulsif entre les atomes de cuivre et les regroupements de nickel. La baisse d'énergie d'activation est le résultat de gradients thermiques qui existent dans la couple de diffusion. Ces gradients sont dus aux différences de résistivités entre les deux éléments.

Pour étudier la diffusion en 3D, un mélange de poudres sphériques de cuivre et nickel a été produit

contenant 5 wt% Cu. Des rondelles faites de ce mélange ont été frittées à des températures de 700, 800 et 900^{o}C pour 30 minutes. Des particules de cuivre isolées ont été trouvées par imagerie d'électrons rétrodiffusés (BSE) et des schémas d'EDS ont été obtenus de la particule et de l'aire qui lui entourait. C'était trouvé que le cuivre a diffusé à travers le nickel de manière uniforme, n'ayant aucuns trajets d'haute diffusion dans une direction spécifique. Les coefficients de diffusion et les énergies d'activation ont été calculés et c'était démontré que la diffusion du cuivre est similaire en direction parallèle et perpendiculaire au courant. En prenant compte les solutions de diffusion binaire et d'homogénéisation de l'expression de diffusion en état non stationnaire, c'était déterminé que le temps requis pour obtenir une répartition homogène de cuivre en SPS surpasse les temps typiques des méthodes conventionnelles.

Contribution of authors

This thesis is written as a collection of two manuscripts: *The effects of applied current on the 1D interdiffusion between copper and nickel in spark plasma sintering* and *Interdiffusion between copper and nickel powders during spark plasma sintering*. The candidate is the primary author of both manuscripts presented in this thesis. Both manuscripts are co-authored by Professor Mathieu Brochu in his capacity as the research supervisor.

In addition, Professor Raynald Gauvin is designated as a co-author of the manuscript titled *The effects of applied current on the 1D interdiffusion between copper and nickel in spark plasma sintering* due to his contribution to the method used for analysis of data acquired by EDS. The Monte Carlo simulation used for correction values of the x-ray intensities was developed and run by Professor Raynald Gauvin. All experiments, data acquisition, and analysis were conducted by the candidate.

Acknowledgements

I would like to thank Professor Mathieu Brochu for his supervision throughout the project and the powder metallurgy research group for their help and advice during the experimentation. I would like to thank Professor Raynald Gauvin, Dr. Nicholas Brodusch, and Jean-François LeBerre for their assistance in the data acquisition by EDS and the analysis of the data obtained.

I would also like to thank AUTO 21 and McGill University for their financial assistance and support throughout the entire project.

Contents

List of Figures

List of Tables

1 Introduction

In the production of complex parts such as those used in automobile production, there is a significant loss of time and material from the machining of wrought components. Powder metallurgy (PM) is an alternative production method for such items. Metal powders are consolidated into a near net shape component which requires very few post production steps [1]. There are many different powder metallurgy techniques, each utilizing different densification and diffusional mechanisms to obtain components comparable to their wrought counterparts in terms of mechanical and physical properties [1]. Conventional PM includes techniques such as press and sinter, where the powder is pressed in a pre-form and then heated to induce consolidation; extrusion, which makes use of a paste composed of the metal powder mixed with certain additives; hot pressing, where pressure is applied on the powder while it is annealed; and many others [1]. Other non-conventional methods are being investigated to reduce production time. One such method is spark plasma sintering (SPS), also known as field-assisted sintering.

SPS is a fairly new PM technique that employs the use of electricity and pressure to consolidate powders [2]. Using the application of an electric field to induce joule heating has been found to reduce sintering time tremendously [3]. Components which take hours to be produced by conventional methods are consolidated within minutes in SPS [2]. Also, with the use of joule heating instead of radiative heating, lower sintering temperatures can be used to obtain the same fully dense and sintered component [3]. This is a result of the temperature gradients generated at the particle contacts caused by the high interfacial resistance. The temperatures at these interfaces are therefore much greater than the overall temperature of the system[3]. In addition, the application of pressure is an asset to producing parts with near theoretical density [3]. The sintering mechanisms at work in SPS are still not well understood. In order to use SPS to its full potential, the effects of the electric field

during sintering must be discerned.

Typically pre-alloyed powders are sintered in SPS. Such powders are quite costly given the extra step required in producing the alloy prior to powder formation. In contrast, the use of blended alloy powders is less costly because they are a mix of a powder of the primary element and a powder made of the alloying elements [1]. In order to obtain a fully alloyed part, all elements must diffuse throughout the component during sintering which is contradictory to the fast sintering kinetics observed in SPS [3]. Therefore, the need for kinetic optimization is required. In order to proceed in this direction, it is important to first understand the diffusional behavior of elements in SPS.

The purpose of this study is to investigate diffusion in 1D and in 3D using copper and nickel as diffusing species. In the 1D case, binary diffusion using bulk materials is studied in SPS and compared to annealing without current to examine the effect of the electric field. To investigate diffusion kinetics in 3D, a powder blend of copper and nickel is consolidated in SPS at various sintering conditions. In order to proceed with this work, diffusion theory and solid-state sintering must first be explained. In addition, the characteristics of SPS, including past studies, and the properties and diffusional behavior of both copper and nickel must be described.

2 Literature Review

2.1 Concepts of Diffusion

Atomic diffusion is the phenomenon which describes movement of atoms within a material. It occurs in order to reduce the energy of the system [4]. The mechanisms through which diffusion occurs within a crystal lattice are substitutional, interstitial, and by surplus of vacancies [4]. Substitutional diffusion occurs when an atom that is at a saddle point, i.e. is not situated at a lattice site but rather free from the vertex formation, moves to a vacancy. Although this occurs in any crystalline material, it is an important mechanism in self-diffusion [5]. Contrarily, interstitial diffusion arises from the presence of solute atoms with a smaller radius than that of those in the matrix. The solute atoms occupy specific sites in between the atoms of the overall matrix [4]. Here, the atomic movement through space can be modeled by considering the flux of the solute atoms. The net flux J in $\mathrm{m}^{-2}\mathrm{s}^{-1}$ of atoms traveling in the lattice is defined by Fick's First Law as,

$$J = -D\frac{\partial C}{\partial x} \tag{2.1}$$

where C is the concentration of the impurity atoms and x is the distance [6]. The parameter D is known as the diffusion coefficient or diffusivity and is a coefficient of proportionality relating the two factors. Because diffusion is a thermally activated process, the diffusivity follows an Arrhenius equation of the form,

$$D = D_0 e^{\frac{-Q}{RT}} \tag{2.2}$$

where D_0 is a pre-exponential factor, R is the gas constant, T is the temperature at which this phenomena is taking place, and Q is the activation energy for diffusion. It can be understood that Q is the energy barrier which must be surpassed in order to allow atomic displacement [4]. In some

cases, the logarithm of the Arrhenius plot of diffusivity is curved and hence the diffusion coefficient is represented by two components. The curve in the Arrhenius plot is due to the presence of a divacancy mechanism. That is to say that atoms diffuse with the presence of two neighboring vacancies [7]. In this situation, two activation energies and pre-exponentials are required, as shown in Equation 2.3, in order to properly describe the system [5].

$$D = D_1 e^{\frac{-Q_1}{RT}} + D_2 e^{\frac{-Q_2}{RT}} \tag{2.3}$$

The probability of an interstitial atom diffusing into a surrounding site is significantly higher than that of a substitutional atom because of the availability of nearby empty sites. Consider the existence of a surplus of vacancies within the system. A vacancy can be considered to have its own diffusivity as a function of the probability of occupying neighboring sites, and there is always an existing possibility for a vacancy to move from one site to another because it is consistently adjacent to at least one atom. Therefore, vacancies diffuse similarly and with the same probability as interstitials. The atom occupying the site of a vacancy, which is diffusing, has the same probability of movement as the vacancy itself. This means of occupation is the mechanism of vacancy diffusion. It follows that vacancy diffusion is expressed in the same manner as interstitial diffusion, following Equation 2.1 as well [4]. A schematic of this process is depicted in Figure 2.1.

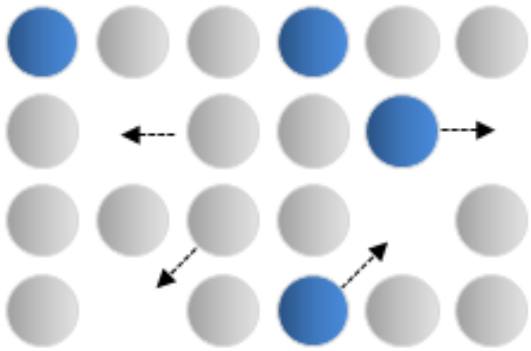

Figure 2.1: Vacancy diffusion between two species.

Equation 2.1 applies to steady state and transient diffusion. An expression to describe non-steady state diffusion must be formulated in order to take into account the effect of time. Consider atoms diffusing from an area of high concentration to one of low concentration. At various points along the

diffusing plane, there is a difference in flux of the diffusing species. Let J_1 be the flux at the distance x_1 and J_2 be the flux at distance x_2. Then, the change in concentration between x_1 and x_2 for a given time step ∂t is as follows.

$$\begin{aligned} \partial C &= \tfrac{(J_2 - J_1)\partial t}{\partial x} \\ \Rightarrow \quad & \tfrac{\partial C}{\partial t} = \tfrac{\partial J}{\partial x} \\ \Rightarrow \quad & \tfrac{\partial C}{\partial t} = \tfrac{\partial}{\partial x}\left(-D\tfrac{\partial C}{\partial x}\right) \\ \Rightarrow \quad & \tfrac{\partial C}{\partial t} = -D\tfrac{\partial^2 C}{\partial x^2} \end{aligned} \tag{2.4}$$

The final expression in Equation 2.4 is called Fick's Second Law [4]. These laws were derived by assuming that atoms diffuse through interstitials, but, as explained previously, vacancy diffusion occurs with the same frequency and probability as interstitial diffusion and hence follows these same laws. The diffusivity D defined in Equations 2.2 and 2.3 is that of a single species diffusing in a matrix. However, if vacancy diffusion in a binary diffusion couple is considered, then the intrinsic diffusivity of a system composed of elements A and B can be calculated by,

$$\tilde{D} = X_A D_B + X_B D_A \tag{2.5}$$

where X_A and X_B are the concentrations of elements A and B at some fixed distance [4]. This parameter is useful when a description of the overall system, including both species, is desired.

The two most commonly used methods for calculating diffusion coefficients numerically are the Boltzmann-Matano (BM) method [8] and the Saue-freise den Broeder (SFB) method [9]. Both are based on the same concept of calculating reciprocal areas of the concentration profile. The BM method requires that the Matano plane be found in order to calculate its diffusion coefficient. The Matano plane, or Matano interface, is that where, on either side, the same amount of each species, in terms of weight fraction, has been diffused [8]. A schematic showing the Matano plane is depicted in Figure 2.2.

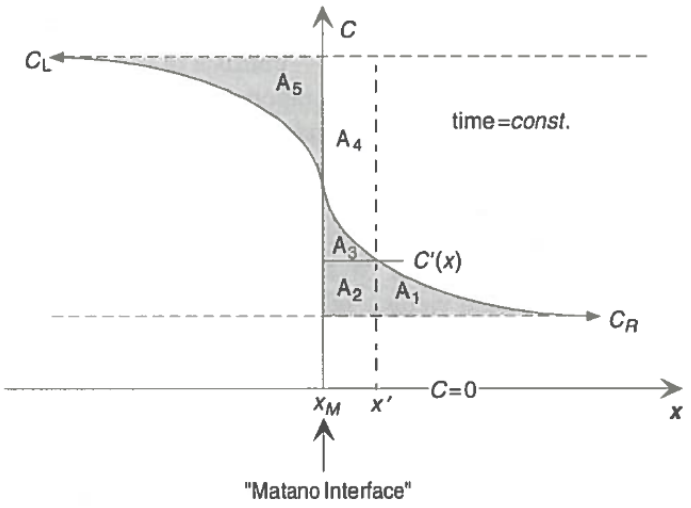

Figure 2.2: Matano interface and the geometry of the Bolztmann-Matano method [10].

The diffusion coefficient at the Matano interface, $D(C')$, can be expressed as the following,

$$D(C') = \left(-\frac{1}{2t}\frac{dx}{dC}\right)_{C'} \int_{C_R}^{C'} (x - X_M) dC \tag{2.6}$$

where C_R is the concentration of the single species at $x = \infty$ and X_M is the Matano interface [8]. The contribution of Boltzmann to this method is in the derivation of Equation 2.6, where the Boltzmann transformation is required in order to eliminate partial differentials from the expression [11]. This method is very widely used, however it requires first finding the Matano plane which is not always trivial.

The SFB method was developed subsequently to remove numerical estimation errors carried on from determining the Matano plane [9]. It calculates concentration dependent diffusion coefficients at any point along the concentration profile. Let $\Psi = \frac{C'-C_R}{C_L-C_R}$ where C' is the concentration at which the desired diffusion coefficient is to be calculated and C_L is the concentration of a species at $x = -\infty$. Then the diffusion coefficient, $D(C')$, is calculated by,

$$D(C') = \frac{1}{2t\left(\frac{dC}{dx}\right)_{x'}}[(1-\Psi)\int_{x'}^{\infty}(C'-C_R)dx + \Psi\int_{-\infty}^{x'}(C_L - C')dx] \tag{2.7}$$

where x' is the distance of C' [9]. The choice of which method to use depends on the apparent

circumstance.

An analytical solution for the resulting differential equation of Equation 2.4 can be calculated in order to obtain a function describing the binary diffusion couple situation. Consider the function $C(x,t)$ describing the concentration of one of the elements as a function of time and space. At $x = -\infty$ for all t, $C(x,t) = 1$ is the starting fractional composition of this element. Similarly, at $x = +\infty$ for all t, $C(x,t) = 0$. Last, it is assumed that at $t = 0$, $C(x,t) = 1$ for $x \leq 0$ and $C(x,t) = 0$ for $x > 0$. Using these boundary conditions, the analytic solution to Fick's Second Law is,

$$C(x,t) = 1 - erf\left(\frac{x}{2\sqrt{Dt}}\right) \tag{2.8}$$

where erf is the error function [6]. As shown in Figure 2.3, the two numerical methods described above generate results at close proximity to the analytical solution.

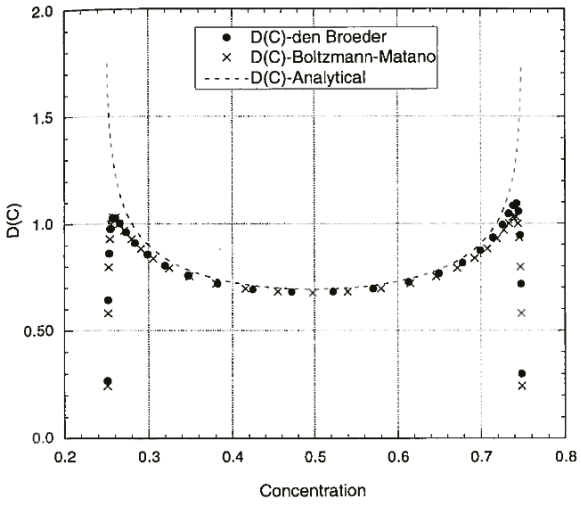

Figure 2.3: Comparison between BM method, SFB method, and analytical solution [10].

So far, the focus has been on the mechanisms of lattice diffusion where atoms are diffusing inside a single grain. However, there are other means of diffusion which may influence the apparent diffusivity of the system. Diffusion along grain boundaries, dislocations, and surfaces are mechanisms that contribute greatly to the overall phenomenon. First, we consider grain boundary and surface diffusion as diffusional mechanisms. Typically, for a fixed temperature, $D_s > D_{gb} > D_l$ where D_s, D_{gb}, D_l are the diffusivities of surface, grain boundary, and lattice diffusion respectively [4]. In

bulk materials, there is more area occupied by grain boundaries than free surfaces, therefore the contribution of the latter is not as important. Nonetheless, in the subsequent section, the effect of surface diffusion will be discussed because there is a large fraction of surface area in powders. As for grain boundary diffusion, the geometry of the material and the dimensions of both the grains and grain boundaries dictate which mechanism is dominant. Given a material with grains of size d and grain boundaries of width δ separating each grain laterally, it can be inferred that the apparent diffusivity is expressed as follows [4].

$$D_{app} = D_l + D_{gb}\frac{\delta}{d} \tag{2.9}$$

In this case, the presiding mechanism is highly dependent on the fraction of area occupied by grains as opposed to grain boundaries. There is, however, little variation in δ in general. Consequently, the highly influential parameter in this geometry problem is that of grain size. The activation energy for diffusion through grain boundaries is significantly lower than that within the lattice, and so, temperature can substantially dictate the dominant diffusional mechanism. Normally, grain boundary diffusion is most relevant below approximately $0.75T_m$ [4]. The case of diffusion through dislocations follows closely that of grain boundary diffusion in that its contribution is also closely related to the geometry. In this case, the dislocations are assumed to be pipes through which atoms can easily diffuse and the relevance of the dislocation diffusion component is related to the cross-sectional area of the pipes. At high temperatures, though, diffusion through dislocations becomes negligible compared to that through the lattice due to the high velocities of atomic movement [4].

The various mechanisms of diffusion play a crucial role in the consolidation of materials in solid state. A very important example of such is sintering of metallic powders to obtain solid parts with features that would be difficult and costly to machine. This results from heat treating a powder compact to temperatures which promote the diffusional mechanisms discussed throughout this section. There exist two methods for consolidation of such powders, solid and liquid phase sintering. In SPS, liquid phase sintering is not possible because liquid inside the die is destructive to the apparatus. Therefore, solid state sintering is the method of interest for this process.

2.2 Solid State Sintering

2.2.1 Sintering Mechanisms

Sintering is the process by which powder particles consolidate together to form a solid part. Heat is applied to the powder in order to overcome the bulk free energy barrier and induce diffusion of the atoms within the particles [1]. During pressure-less sintering, deformation and consolidation occurs in three stages as shown in Figure 2.4.

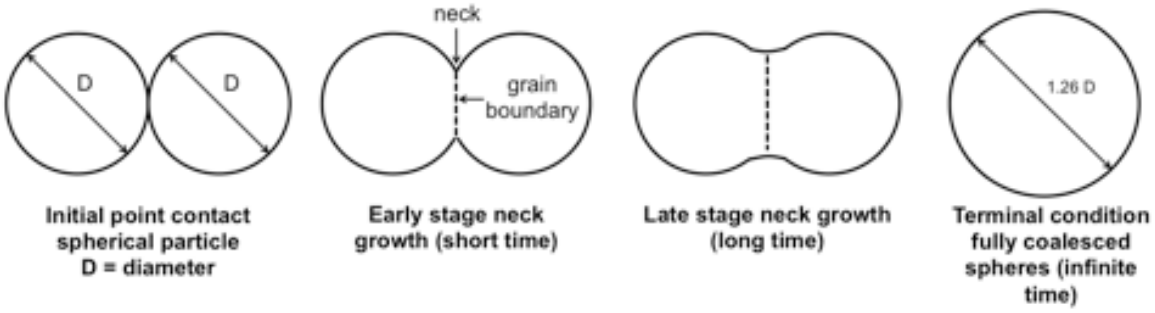

Figure 2.4: Neck growth during sintering [1].

However, in SPS and the analogous conventional method of hot pressing, pressure is applied during sintering which quickens the neck formation process and changes pore geometry [1]. There exist various sintering mechanisms dependent on, amongst other properties, the temperature at which the process is being performed. Volume and grain boundary diffusion were discussed in the previous chapter. Here, another diffusion type is present, that of surface diffusion. Surface diffusion occurs at low sintering temperatures where the atoms along the surface of the particles are displaced in order to form the neck and encourage its growth [1]. This mechanism does not contribute to shrinkage or densification and, during pressure-less sintering, results in high porosity [1]. The overall bulk diffusion is comprised of volume and grain boundary diffusion where atoms inside the particles are transported to the necking areas. As a result, the particles themselves shrink and, as atoms diffuse, the neck itself grows causing the ensemble to densify and form one solid component [1]. These mechanisms, which are seen at moderate to high sintering temperatures, are essential in obtaining a highly dense product with minimal porosity [1]. The difference between bulk mass transport and surface transport can be seen in Figure 2.5.

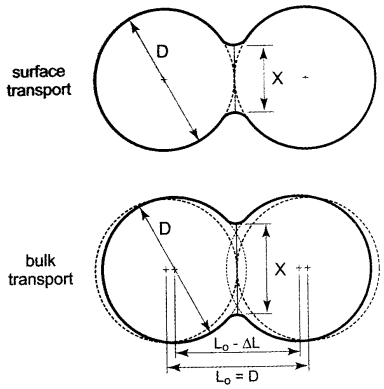

Figure 2.5: Bulk diffusion vs Surface diffusion [1].

2.2.2 Sintering Practices

Conventional sintering practices vary depending primarily on the desired final product and the materials being sintered. For the purposes of this work, the focus is on sintering of metallic powders, although, many different types of materials can undergo these processes for piece fabrication. To start, powders can either be compacted prior to sintering or during the heating process. Compaction before heating can be done in air and usually involves the use of a hydraulic press to plastically deform the powder particles and create interlocks between them [1]. During the annealing step, various surrounding environments can be chosen. The choice of which is mostly a function of the possible reactions that can occur during sintering. For example, if the formation of oxides is a possibility, then sintering in air is not favorable. The same can be said for nitrides, carbides, etc. Sintering in vacuum is also largely practiced and is the only method which yields a final product with full density [1]. Regardless of technique, it is always optimal to attain temperatures of approximately $0.7T_m$ where T_m is the melting temperature of the material [1].

A variety of different powder consolidation and sintering methods were mentioned during the introduction of this project. Due to its similarities with SPS, emphasis will be put on the process of hot pressing. This method is characterized by the use of a heated die and heated punches during compaction of the powder. This produces a consolidated part immediately after removal from the die. The densification mechanisms at work during hot pressing are creep, plastic flow and thermal diffusion [1]. The effect of thermal diffusion is clear from the process of neck development explained

previously. Plastic flow is caused by the application of pressure during the process. Deformation of the powdered material is important to ensure high contact areas between particles and remove porosity. During heating and throughout the compaction hold, as a deformation mechanism, creep contributes in some part to atomic movement [12].

Creep is a stress induced deformation mechanism. It is present in hot pressing due to the application of pressure. At high temperatures, power-law creep, defined as rate-dependent plasticity, is the type to be considered. Over $0.6T_m$, randomly distributed dislocations can climb as well as glide and, above $0.6T_m$, these climbs are controlled by lattice diffusion [12]. Atomic movement from dislocation climb contributes to the overall lattice diffusion and therefore is included in expressing the effective diffusivity. Given that lattice diffusion is a key component in densification during sintering, power-law creep, by it's contribution to lattice diffusivity, is also a factor in consolidation between powder particles. Now, while densification implies pore removal during sintering, here consolidation is used to denote the joining of particles through necking. Atomic movement by power-law creep is depicted in Figure 2.6.

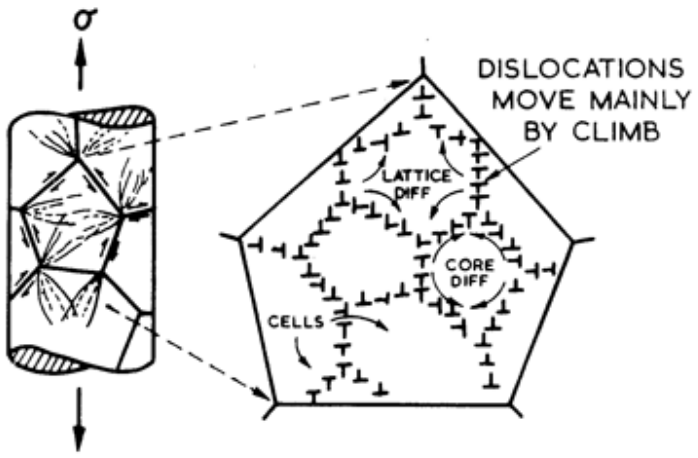

Figure 2.6: Power-law creep due to dislocation climb [12].

The derivation of an expression for effective diffusivity including the effects of dislocation movement was derived by Hart,

$$D_{eff} = (\bar{l^2}/2\tau)f + D_0(1-f) \tag{2.10}$$

where τ is the time at which an atom spends at a dislocation, $\bar{l^2}$ is the mean square projected

distance it travels during this time, f is the fraction of atoms in dislocations, and D_0 is the volume diffusion coefficient [13]. This expression demonstrates that in order to properly model diffusivity, diffusion through dislocations must also be considered. This effective diffusivity can be used to model atomic diffusion and ensure proper distribution of elements during hot pressing.

Spark plasma sintering is an alternative to conventional hot pressing which promotes short sintering times and develops fully dense products. While hot pressing requires sintering times on the scale of a few hours [1], SPS can produce consolidated parts within minutes [2].

2.3 Spark Plasma Sintering

2.3.1 The Spark Plasma Sintering Method

Spark plasma sintering mimics hot pressing, but is differentiated by the use of a pulsed D.C. current to induce consolidation of powders. The use of current to induce joule heating was first developed in the 1960s in Japan and has since evolved into the modern SPS technique used today [14]. Much research has been attributed to SPS due to the possibility of obtaining high heating rates resulting in shorter sintering times and the constant application of pressure which aids in producing fully dense consolidated pieces [3]. These two properties also limit grain growth during sintering, which is especially favorable for consolidating nano-grained materials [15]. The machine itself functions as follows, the powder sample is placed inside a die in between two punches, all made of conductive material. This assembly is then placed inside a vacuum chamber and a pulsed D.C. is applied through the punches and the die. Simultaneously, a hydraulic press is used to apply pressure which exerts compressive force on the specimen inside. The entire system is water cooled and argon gas is used to relieve the vacuum once the procedure has finished. All settings, including the desired sintering temperature and times, the length and frequency of the pulse, etc. are adjusted using a control system linked to the machine. A schematic diagram of the SPS configuration is shown in Figure 2.7.

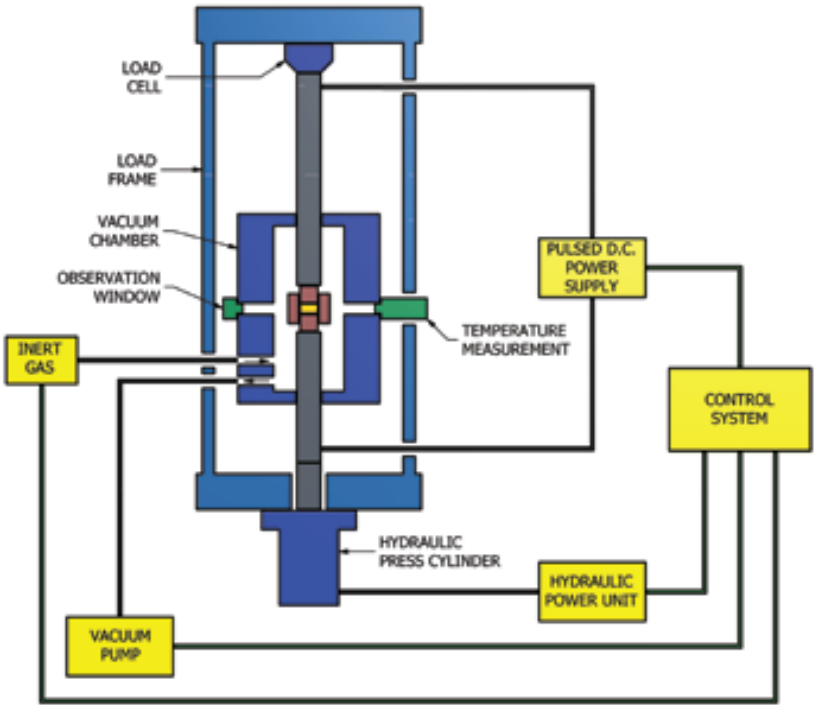

Figure 2.7: Schematic diagram of spark plasma sintering configuration [2].

Consolidation occurs as follows, the application of pressure compacts the powder and ensures high contact area between the particles. Simultaneously, the current passes through the particles and encounters points of resistance at the particle contacts. Joule heat is generated at these contact points inducing necking [2]. Figure 2.8 depicts the path taken by the current when passing through a powder.

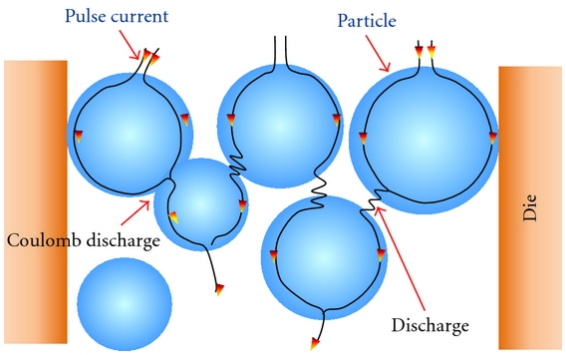

Figure 2.8: Current path through powder particles in SPS [16].

For an extended period of time, it was believed that the increased heat at the contacts caused a

spark or discharge and melting resulting from the presence of plasma at the particle surface, hence the name spark plasma sintering. However, later studies showed that in fact there is no discharge nor production of plasma at the contact points because the voltage applied is too low and the process is performed in vacuum [17–20]. Hulbert *et al.* demonstrated the absence of plasma through in situ atomic emission spectroscopy [19, 20]. This method allowed visual observation of any possible plasma or spark appearance. Voltage measurements were also taken between both punches to detect any observable radiation anomalies. After numerous experiments where many different parameters were varied, it was concluded that there is no plasma nor sparking produced in SPS [19, 20].

The three important aspects that characterize SPS and make it an interesting prospect for the field of powder metallurgy are the high heating rates generated, the electric field effect, and the application of pressure during sintering.

2.3.2 Effect of High Heating Rates

High heating rates are a characteristic of SPS that demonstrate its improvement over conventional sintering. Like hot pressing, the die material used is normally thermally conductive so that, given that the die is in direct contact with the green body, it can also act as a radiative heat source [21]. In SPS, overly high heating rates arise from joule heating generated by the resistance between particles. These peaks in temperature can also give rise to cleansing of the particle surfaces from impurities or oxides which again aids in accelerating the sintering process [15]. The removal of these layers of oxides and impurities allows grain boundaries, originating from particle interfaces, to act as high diffusing paths which increases the diffusion velocity and consequently quicken neck development [22]. Given that the heat arises from contact resistance between particles, there exist inhomogeneous temperature gradients throughout the green body. Attempts to model these gradients were done by Vanmeensel *et al.* [23]. It was shown that horizontal contacts with the graphite are a source of resistance and can reduce thermal conductivity at these points. In practice, the horizontal contact points are the surfaces of the powder compact that are in contact with the punches. On the other hand, resistance due to the vertical graphite surface is significantly greater and causes

a much larger decrease in thermal conductivity. This is due to the lower quality contact between the graphite paper and the die compared to the contact with the horizontal punch that is applying pressure on the specimen throughout the process. Finally, it was shown that for conductive materials the temperatures near the edges of the powder compact are lower than those near the center [23]. Given that temperature can only be measured externally in SPS, this creates discrepancies in its overall evaluation throughout the system. These radial temperature differences were confirmed by Zavaliangos *et al.* with similar finite element modeling [24] and were subsequently reproduced by Yucheng *et al.* and Molénat *et al.* using different conducting materials such as TiB_2 and TiAl respectively [25, 26]. Comparisons were made by these authors between the radial temperature differences in conducting materials and insulating materials and it was shown that high temperature gradients occur from the center of the specimen outwards in conductive materials while the opposite is true for insulating materials [23–26]. Modeling of the radial temperature distribution performed by Vanmeensel can be seen in Figure 2.9.

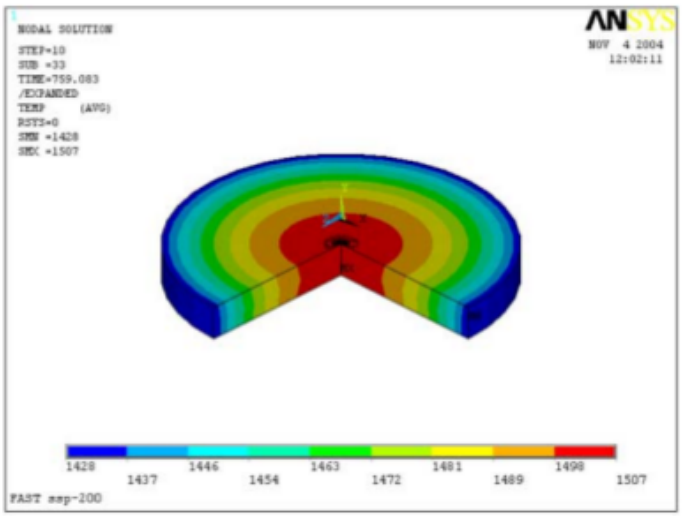

Figure 2.9: Temperature distribution of 40 mm diameter electrically conductive TiN sample sintered by SPS [23].

While Vanmeensel, Zavaliangos, and Yucheng performed experiments using ceramics [23–25], which, even though they are conductive, still have higher resistivities than metals, Molénat studied the temperature inhomogeneity in SPS using TiAl whose resistivity of $4.06 \times 10^{-7}\Omega$m [27] is comparable to that of copper. It was shown that there is still a large discrepancy between the temperature at the center of the sample in comparison to the die wall and further to the point at which

a pyrometer can be placed [26]. Experiments were performed at two separate voltages and the results of the calculated radial temperature from the center of the specimen to the outside of the die are shown in Figure 2.10.

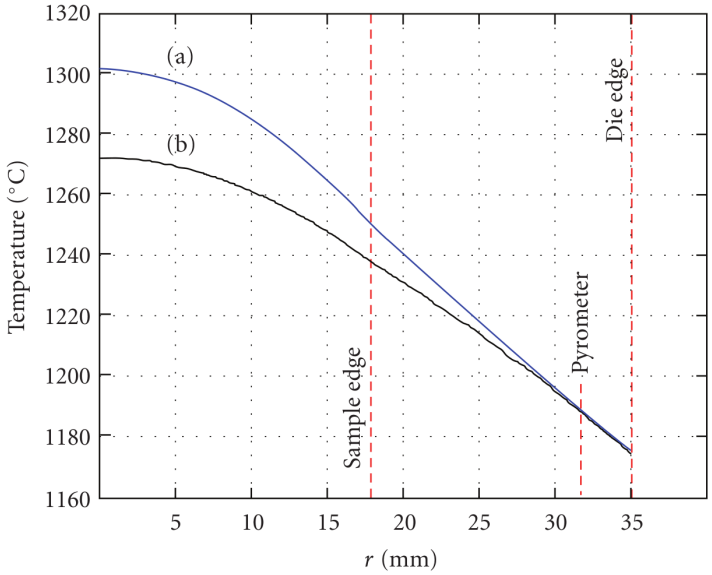

Figure 2.10: Radial temperature variation of TiAl for experiments performed at (a) 4.2 V and (b) 2.85 V [26].

It was also seen that the pressure applied can affect the temperature distribution inside the punch and die set-up by improving the punch/die contact [28]. Higher pressures of 80 MPa were found to reduce the difference in temperature distribution due a greater outward force created between the punches and the die, which improves surface contact [28]. This caused improved conductivity throughout the entire system [28].

One of the most important attempts on modeling temperature distribution and the effect of high heating rates in SPS was performed by Olevsky *et al.* [29]. This was studied as a component in the overall modeling of densification in SPS. The contribution of thermal diffusion to densification was modeled as follows. First, the following formulation of the vacancy flux due to thermal diffusion is used.

$$J = -D\frac{\kappa_T}{\langle T \rangle}\nabla T \tag{2.11}$$

Here, D is the diffusion coefficient, $\langle T \rangle$ is the spatial average temperature, and $\kappa_T = \frac{C_v H_m}{k\langle T \rangle}$ is the

thermal diffusion ratio where C_v is the vacancy concentration and H_m is the enthalpy of vacancy migration [29]. This formulation takes into account the non-uniformity of the temperature distribution inside a powder sample. Now, the driving force of vacancy migration is the divergence of the flux. This value is computed to ensure a lower bound for when thermal diffusion has an impact on the shrinkage rate. After considering the expression for average temperature gradients given the presence of pulsing derived by Gostomel'skii *et al.* [30], shrinkage due to thermal diffusion during pulsing was derived as a component of the entire constitutive model of deformation and shrinkage in SPS [29]. It was further deduced that local temperature gradients can be significantly higher than the overall macroscopic temperature distribution and that these gradients highly affect vacancy migration [29]. These expressions serve as a good basis for a shrinkage model that includes thermal diffusion in SPS and are also very helpful for any rapid sintering technique.

2.3.3 Effect of Applied Current

The next important characteristic of SPS is the application of current during sintering. Apart from inducing joule heating and creating high temperature zones at contact points, the applied current produces an electric field which adds to the driving forces in SPS. A base model was derived by Olevsky *et al.* in which the contribution of electromigration to the shrinkage by grain boundary diffusion is expressed by the following,

$$\dot{\varepsilon}_{gb}^{em} = \frac{\delta_{gb} D_{gb}}{kT} \frac{Z^* e}{(G + r_p)^2} \frac{U}{l} \tag{2.12}$$

where U is the electric potential and l is the characteristic length along the electric field [31]. Atomic movement due to electron wind is assumed negligible in SPS due to the lack of high current densities. Therefore, Equation 2.12 is a description of the interactions between grains, grain boundaries, and pores that are affected by the electric field. Olevsky's definition of electromigration is not in the conventional sense but describes the driving force of the electric field causing movement of the atomic nuclei towards the cathode. The lack of consideration of the electron wind is further established by neglecting the magnitude of the current, the main artifact dictating electromigration of ions, and considering electric potential as a component to the expression. Many studies have been performed to observe the effects of the electric field in SPS on varying material properties [22, 32–

35], and overall final microstructure and properties are comparable to conventional processing. In some cases, it has been shown that consolidation with SPS can improve mechanical properties. For example, Zhang *et al.* demonstrated through the consolidation of nanocrystalline copper that yield strength could be increased to 650 MPa when optimal sintering parameters were used [36]. Given that proper choice of sintering parameters is imperative, it is important to consider the role of the pulse in sintering with SPS. Spatial changes in electric current and voltage were studied and the results led back to the proper choice of sintering material and die material [37]. On the other hand, changing pulse frequency, although this led to a decrease in resistivity with increasing pulse frequency at the initial stages of sintering [38], showed no difference in final material properties such as tensile strength and density [39, 40]. Hence, the role of the pulse D.C. in SPS is in generating the peak temperature points at the particle contacts and creating the joule heating needed to induce sintering. Pulse is used instead of constant D.C. to lower the average power output required in attaining the desired high current densities.

2.3.4 Effect of Applied Pressure

Analogous to hot pressing, in SPS the punches apply a constant uniaxial force on the powder specimen inside the die during heating. This ensures interlocking and the creation of high contact areas between particles which promotes joule heating in all areas of the specimen. Applying an external load also causes particle rearrangement, which ensures optimal packing and destroys agglomeration [3]. With the application of pressure, pores are easily removed allowing full density to be obtained more rapidly than sintering in a vacuum environment alone [3]. Sintering can also be performed at lower temperatures than standard practices while still obtaining a fully sintered and densified final piece [3]. The contribution of pressure is, however, highly dependent on particle size [3]. When particles are small, the pressure effect is small, and as particle size increases, so does the pressure's contribution to the overall driving forces [3]. This reaches a peak of optimal particle size to pressure effect. When the particle size becomes too large, the contribution of pressure becomes small again because there is less rearrangement [3]. The relation of the intrinsic driving forces for

sintering and the contribution of pressure to these driving forces is represented by Equation 2.13.

$$\frac{d\rho}{(1-\rho)dt} = B\left(g\frac{\gamma}{x}+P\right) \tag{2.13}$$

Here, ρ is the fractional density, t is time, B is a constant taking into account diffusivity and temperature, g is a geometrical constant related to particle size, γ is the surface energy, P is the external pressure, and x is a scale parameter also related to particle size [3]. By the above equation, it is seen that the critical point where the contribution of the external load to the driving forces for diffusion is high is when the pressure is equal to $g(\gamma/x)$, a parameter of the particle size. In a first effort to characterize particle coalescence in SPS, an expression for shrinkage rate of grains, grain boundaries and pores during compression and sintering of a powder was formulated by Olevsky *et al.* [31]. This was derived as another component in the formulation of overall shrinkage. The contribution to grain boundary diffusion of the external load is of the following form,

$$\dot{\varepsilon}_{gb}^{dl} = \frac{\delta_{gb}D_{gb}}{kT}\frac{\Omega}{(G+r_p)}\frac{\bar{\sigma}}{G^2} \tag{2.14}$$

where δ_{gb} is the grain boundary thickness, D_{gb} is the grain boundary diffusion coefficient, G is the grain size, r_p is the pore radius, Ω is the atomic volume, and $\bar{\sigma}$ is the effective external stress [31]. This expression describes horizontal shrinkage, that is, along the long edge of the grain. This reinforces that grain size plays a large role in the magnitude of the contribution of applied pressure. Since shrinkage is proportional to the inverse of G^2, it is seen that large grains cause less shrinkage. There is a greater ease in re-arranging smaller grained materials which aids in increasing the shrinkage rate. On the other hand, pressure alone is not sufficient to ensure proper sintering of a material. Experiments performed by Diouf *et al.* showed, with the use of copper powder, that without adequate temperature, the final product obtained from SPS would be fully dense but not fully sintered [41]. During heating, the application of pressure was responsible for different displacement phenomena a different temperatures. At low temperatures, constant pressure causes rearrangement of the particles to form a closely packed compact [41]. Above 200^{o}C, the application of pressure caused local deformation of the particles and resulted in near full density. However, even though near full density was obtained, full sintering was not. It is only after a threshold tem-

perature where the application of pressure induces core deformation promoting large densification and complete sintering in the final product [41]. It is seen in Figure 2.11 that the temperature at which the highest displacement rate is observed is between 500^{o}C and 600^{o}C which is well bellow the average sintering temperature for a pressureless or pre-compaction approach for this material [41].

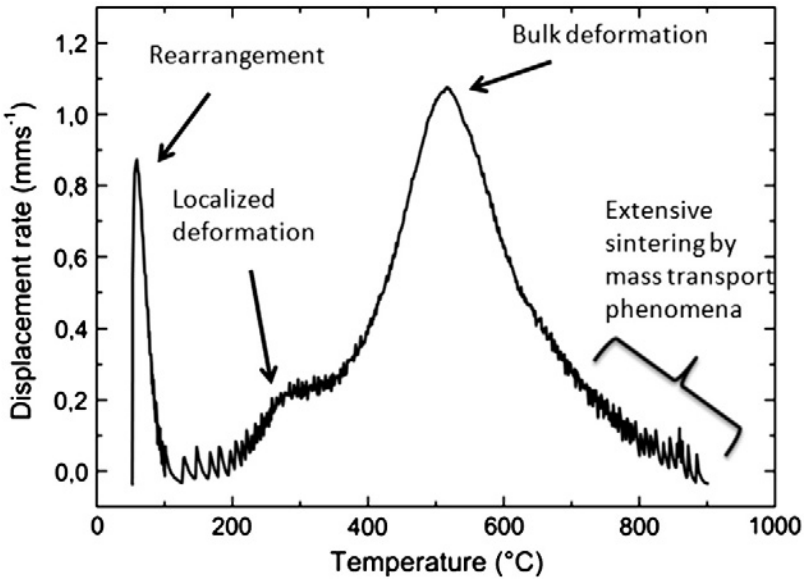

Figure 2.11: Displacement rate as a function of sintering temperature [41].

This demonstrates that the application of pressure ensures maximum densification prior to mass transport and neck development and that sintering begins after peak deformation has occurred [41]. It is important to note that without pressure, obtaining full density is still a possibility because materials are sintered under vacuum in SPS. However, the time required for such a procedure is impractical. This, along with ensuring proper current paths, are the reasons why pressure is a necessity in consolidation by SPS.

Hot pressing is used as a direct comparison to SPS because of the attributes and densification mechanisms they share. However, one of the most important differences between SPS and conventional sintering is the presence of an electric field. The applied current induces joule heating at particle contacts by generating current densities proportional to the desired sintering temperature. It has been stated that the lower bound for an applied current to cause electromigration is 10^3 A/cm^2 [42], which is near the range of possible current densities that can be used in SPS. Therefore, it

must be investigated as to whether electromigration occurs in SPS.

2.4 Electromigration

Electromigration is mass transport induced by the application of current. In a conductive material, there exist two opposing forces when current is applied. The first is the electric field from the cathode to the anode and the other is the momentum generated by collisions between the electrons of the electron wind and the positive ions in the material [43]. Metal bonds result from the existence of an electron cloud surrounding the positive nuclei positioned at the vertices of the crystal lattice [44]. When current is applied, the electrons in the cloud with sufficient energy to enter the conduction band are displaced [44]. Therefore, when it is said that an atom has undergone collisions with the electron wind, it is the atomic nucleus, a positively charged ion, that is the actual object taking part in this event [44]. During the application of current through a conductor, the shielding positive ions reduce the force of the electric field in the forward direction. Therefore, the effect of the electron flow is usually predominant [43]. Consequently, in vacancy diffusing species, ions upstream from vacancies with respect to the electron flow will have higher probabilities of occupying said vacancies [43]. This increase in probability of vacancy occupation is due to the lowering of the energy barrier for atomic movement. When the electrons collide with the positive ions in the conductor, their momentum energy is transferred to these ions. This increases the atom's kinetic energy and causes a decrease in the required activation energy for diffusion [43]. A schematic depicting electromigration is found in Figure 2.12.

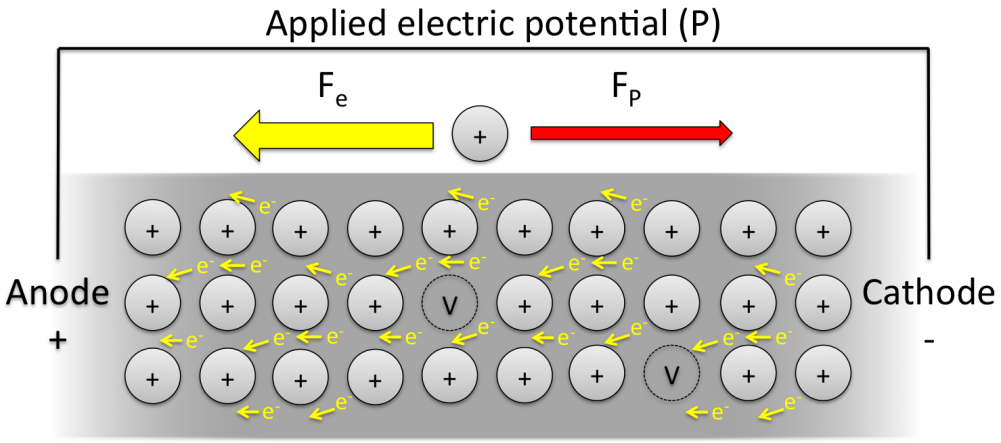

Figure 2.12: Current induced forces in conductive material [45].

In regions where positive or negative gradients exist, voids and hillocks can be observed [43]. These can be temperature, current density or concentration gradients. In areas of negative gradients, ions are accumulated downstream from the electron flow because there is insufficient vacancy movement to ensure their removal. In this case, hillocks or whiskers can be observed throughout the specific part of the material [43]. Conversely, areas of high gradients allow for large movement of vacancies. These vacancies can accumulate if they are not annihilated quick enough and create sinks, which grow into voids or pores [43]. Prior to the formation of hillocks and voids, there is an increase in stress gradients caused by the electric field [46]. In thin films, Blech described the existence of a critical film length such that below it, there is no noticeable effect of electromigration arising from these stress gradients [47]. At such short film lengths, the stress induced by the electric field counters that of the electron wind which results in a backflow and zero net movement of the atoms [47]. The relationship between the existing types of gradients and the conductor length are shown in Figure 2.13.

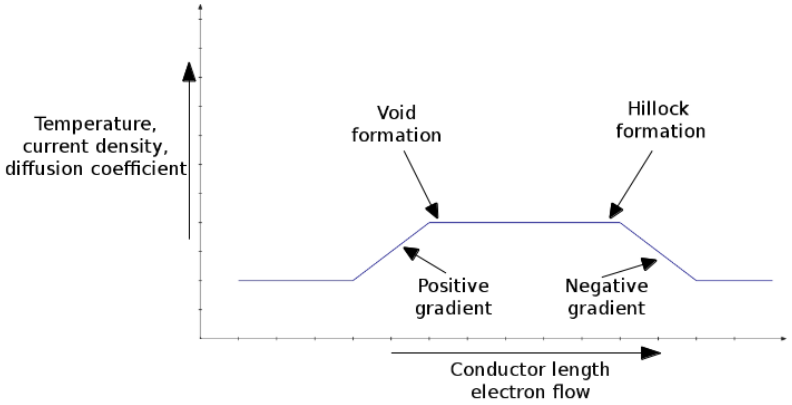

Figure 2.13: Schematic of void and hillock formation [43].

There is a similar relationship involving the applied current density and atomic drift due to electromigration, where the two are inversely proportional to each other. When the inhibition of movement is caused by the current density, the increased stress is due to elastic storage of the ions and the creation of hillocks by over saturation [47]. To summarize, when high current densities are applied to a material, the electromigration induced vacancy diffusion is driven by the electron flow, stress gradients caused by both the electric field and the occupation of a vacancy by an atom of greater size, temperature gradients from joule heating, and vacancy concentration gradients or, synonymously, chemical potential gradients. [48].

The drift velocity attributed to electromigration, v_{ef} is defined by the following equation.

$$v_{ef} = \left(\frac{D}{kT}\right) eZ^{*}\rho j e^{-\Delta H/kT} \tag{2.15}$$

Here, D is the effective diffusion coefficient, T is the annealing temperature, e is the charge of an electron, Z^{*} is the effective charge of the material, ρ is the resistivity, j is the current density, ΔH is the activation energy, and k is Boltzmann's constant [49]. It is seen here that the important parameter to consider for electromigration induced drift is the current density. It has been shown that minimum current densities between $10^3 - 10^5$ A/cm^2 are required to observe any effects due to electromigration [42, 50].

Since many applications of the work done on electromigration are in electronics, more often than not the current applied is in the form of a pulse. This is also true in SPS. Experiments with pulsed applied current usually decouple the process by considering the ON-time and OFF-time. During the ON-time, the driving forces for electromigration induced diffusion are those listed above with the chemical potential and stress gradients acting in the opposite direction of the electron flow [51]. The temperature gradients can be in either direction depending on the system. During the OFF-time of the pulse, the electron wind driving force is no longer present and all that is left are the forces leading in the opposing direction [51]. The opposing driving forces during pulsed D.C. are depicted in Figure 2.14.

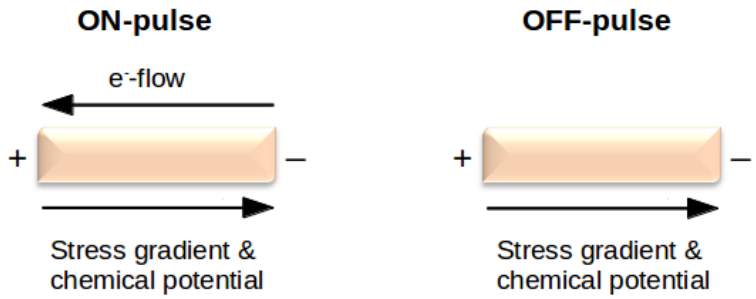

Figure 2.14: Opposing driving forces during pulse applied current.

This creates a backwards transport of material unlike the backflow described by Blech [47] because this phenomenon is seen in bulk material components that surpass the Blech critical length. As an example, the effects of pulse induced backflow can be seen when a pulsed direct current is passed through a material containing precipitates. These precipitates will accumulate at the anode when they are transported by electromigration but will then dissolve back into the matrix when current is turned off [52]. Overall, it is seen that interconnects have much longer lifetime and longer time to failure with a pulsed D.C. than continuous current [51, 53, 54].

2.5 Copper and Nickel Interdiffusion

The copper nickel system is an attractive system to work with because the two form a complete solid solution with no presence of intermetallics. These species have been chosen for this work because they are the textbook example of a diffusion study. The phase diagram of these two elements is

shown in Figure 2.15.

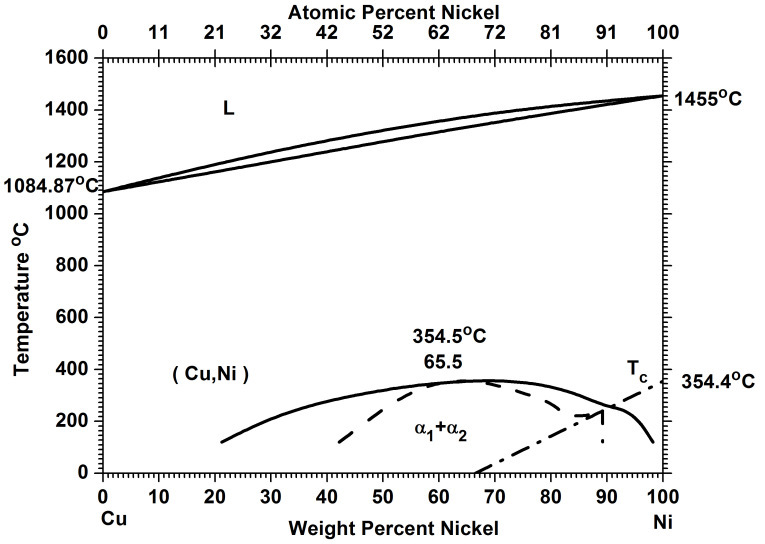

Figure 2.15: Cu-Ni phase diagram [55].

The two form an FCC solid solution at fairly elevated temperatures for all fractional compositions. There is a miscibility gap observed at 354.5^{o}C composed of two FCC phases of each of the pure elements. This phase has been proven to exist through thermodynamic calculations [56] and through neutron diffraction experiments [57, 58] however, conventional metallographic methods are unable to do so [59]. Table 2.1 demonstrates how the Cu-Ni system is a model for diffusion experiments by their physical and chemical properties.

Table 2.1: Physical properties of Cu and Ni [5].

	Atomic Radius (pm)	Resistivity at 20^{o}C ($\mu\Omega$cm)	Thermal conductivity at 20^{o}C (W/mK)	Electronegativity
Cu	128	1.694	397	1.9
Ni	124	6.9	88.5	1.91

On their own, each element is arranged as face-centered cubic and, due to the similarity in atomic radii, the diffusion mechanism at work in this system is vacancy diffusion [6]. The nearly identical electronegativity values ensure excellent mixing between copper and nickel, and, as a result, allow the formation of a complete solid solution.

Interdiffusion between copper and nickel can be studied through several outlets, thin films, radioactive tracers, and bulk diffusion couples. Each show different diffusional properties due to the material structure in each case. For example, grain boundary diffusion is a greater contributer to the effective diffusivity in thin film couples due to the high grain boundary density. Also, in thin films, diffusion through defects, such as dislocations, is a non-negligible diffusional mechanism, which increases the overall diffusivity of the system [60]. In bulk material there may still be a strong grain boundary component if the grains are of an appropriate size. For example, at 500^{o}C, grain boundary diffusion can be predominant with grains up to 80 μm [61]. As mentioned in the section on diffusion theory, the apparent diffusivity is the sum of grain boundary and bulk diffusion where the size of the grains and the width of the grain boundaries dictate the weight of the grain boundary diffusion term. However, temperature still plays a large role in the contributions of either mechanism. It was shown by Krishtal *et al.*, in copper and nickel diffusion couples, that at high temperatures, such as 700^{o}C and 800^{o}C, volume diffusion is the predominant mechanism for even small grained solids (15 and 35 μm respectively) while at low temperatures similar to that stated in the above example, grain boundary diffusion is a significant contributor even when large grains are present [61]. It is, therefore, important to consider literature values for volume diffusion of copper and nickel at high temperatures to remove any contribution of grain boundary diffusion to the effective diffusivity. In fact, in copper, if diffusion is performed at temperatures greater than $0.6T_m$, grain boundary diffusion can be considered negligible and an appropriate value for volume diffusion can be calculated [62].

At the atomic level, copper and nickel diffuse into each other through different types of vacancies. While copper atoms transport through conventional single vacancy diffusion, nickel diffuses through divacancies [7]. It was mentioned earlier that if the Arrhenius plot of diffusivities is curved, then there are two activation energies and pre-exponential factors to be considered. This occurs in nickel and is the case of divancancy diffusion. Divacancies occur as soon as vacancies become mobile or are in the collision cascade [63]. They are a result of small energy gains and entropic tendencies when two vacancies appear at neighboring lattice sites [10]. This phenomenon is mainly seen in FCC metals although it can manifest itself in other crystal structures as well [63]. During diffusion of nickel into copper, the contribution of divacancies becomes very significant and creates uncertainties and increased absolute error during calculation of the diffusion coefficient. The increase in uncertainty

arises from the requirement of two activation energy and pre-exponential components to calculate diffusivity. The contribution of monovacancies and divacancies must be determined separately and these two artifacts depend on temperature in different ways [10]. While single vacancies have a constant weight in the magnitude of the diffusion coefficient throughout wide temperature ranges, the contribution of divacancies to diffusivity increases with increasing temperature [7]. This is because divacancies, with their dependence on entropy, become a significant contribution to diffusion at temperatures that cause high atomic mobility, such as near the melting point [10]. Due to the complication of describing diffusivity when divacancies are present, it is more favorable to track the diffusion of Cu during experimentation of Cu and Ni diffusion couples.

The experiments used for calculating diffusion coefficients involve using a tracer element within a bulk specimen, normally at fairly high temperatures. Determining interdiffusion coefficients in bulk specimens requires different methods such as tracking either element in an alloy composed of the two. In Table 2.2, the pre-exponential and activation energy for copper diffusing in nickel were calculated by means of a thin film layer of copper deposited on a nickel substrate. The sample is then cut and the penetration of copper into the bulk nickel is calculated [64]. The diffusion of nickel in copper was determined by data fits of various sources [65–67] in order to isolate the contribution of both the monovacancies and divacancies [5].

Table 2.2: Pre-exponential diffusion factor and activation energies for both directions in a copper and nickel diffusion couple.

	D_0 (cm^2/s)	Q (kJ/mol)
Cu→Ni [64]	0.61	255
Ni→Cu [5]	$D_{01} = 0.7$	$Q_1 = 225$
	$D_{02} = 250$	$Q_2 = 299.3$

As will be seen during the experimental portion of this work, diffusivity varies with concentration. Therefore, it is important to track diffusivity coefficients throughout a range of concentrations in order to properly assess interdiffusion. Data obtained by Heumann *et al.* is shown in Figure 2.16.

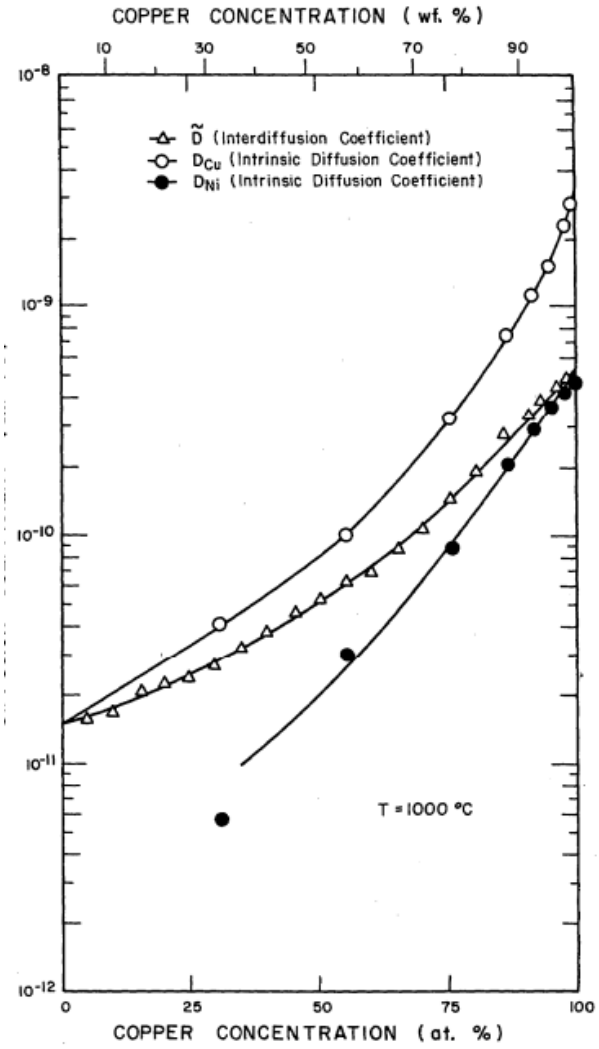

Figure 2.16: Diffusivities of Cu and Ni as a function of Cu concentration [68].

These experiments were performed using an electron microprobe and the Matano method for calculating diffusivities [68]. Experiments were performed at 1000^{o}C to ensure minimal contribution of grain boundary diffusion. The increase in the trend results from the relation between diffusivity and the concentration gradient. At high copper concentrations, there is increased mobility towards regions depleted of copper which results in a high concentration gradient and high diffusivity. Other investigations performed by Brunel *et al.* to determine the interdiffusion coefficient, $\tilde{D}$, of copper and nickel are shown in Figure 2.17 [69]. Again, an electron probe was used for data analysis. Here, the Matano method was used after analytical calculations of diffusion penetration. Their results were compared with experimental data taken from the use of radioactive tracers and conventional bulk

diffusion couples [70].

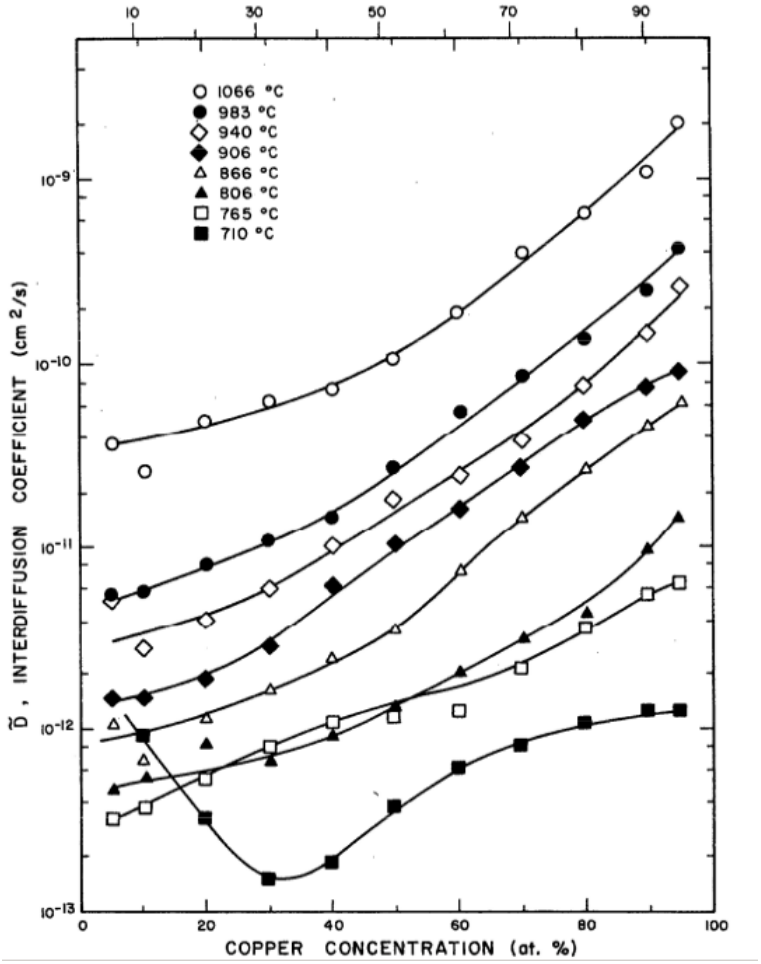

Figure 2.17: Interdiffusion coefficients calculated by Brunel *et al.* at varying temperatures and copper concentrations [69].

3 Experimental Methods

3.1 Project Overview

Diffusion in SPS was studied through two routes. First, an assessment was carried out in 1D by the use of bulk material and, subsequently, diffusion in 3D was studied using blended copper and nickel powders. The structure of this work is as follows.

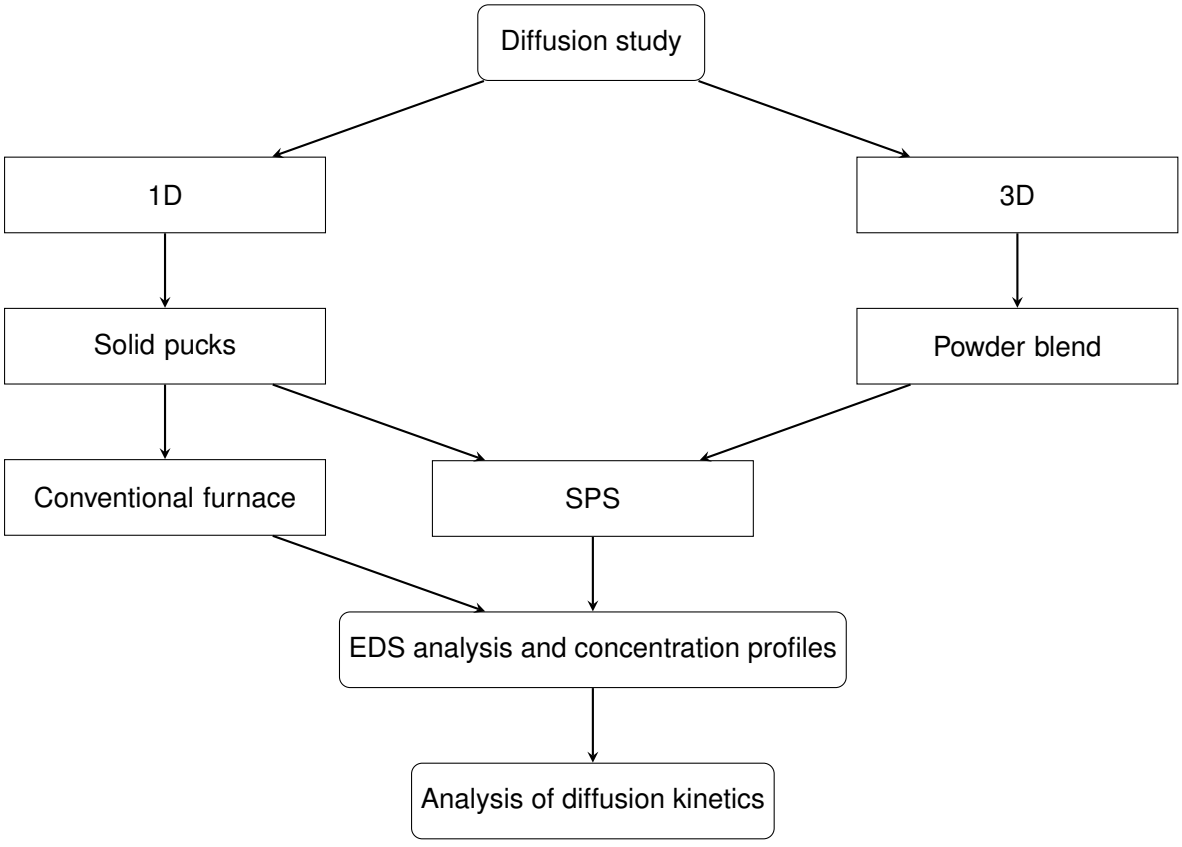

3.2 Sample Preparation

3.2.1 1D experiments

Copper rods of 99.99% purity and nickel rods of 99% purity, both with 3/4 inch diameters were obtained. These rods were sectioned into cylindrical pucks 20 mm in diameter and 5 mm in width. One face of each puck was ground using 320, 600, and 800 grit grinding paper and then polished with 9 μm, 6 μm, and 1 μm monocrystalline diamond suspension. These were then cleaned with water, soap, and acetone. The final prepared pucks are shown in Figure 3.1.

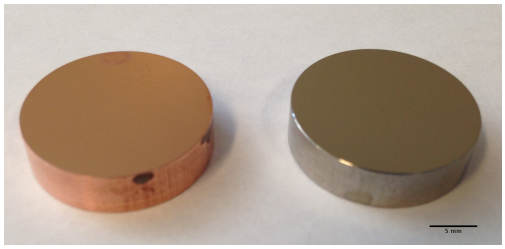

Figure 3.1: Polished copper (left) and nickel (right) pucks.

For a single experiment, one nickel puck and one copper puck were placed in a Thermal-Technology SPS press with the polished faces adjacent to each other. Experiments were performed with two orientations, one where the copper puck is placed on top of the nickel puck, denoted Cu/Ni, and the other where the copper puck is placed beneath the nickel puck, denoted Ni/Cu. A schematic of both configurations is shown in Figure 3.2. In all cases, the inside of the die and punches were covered with graphite foil.

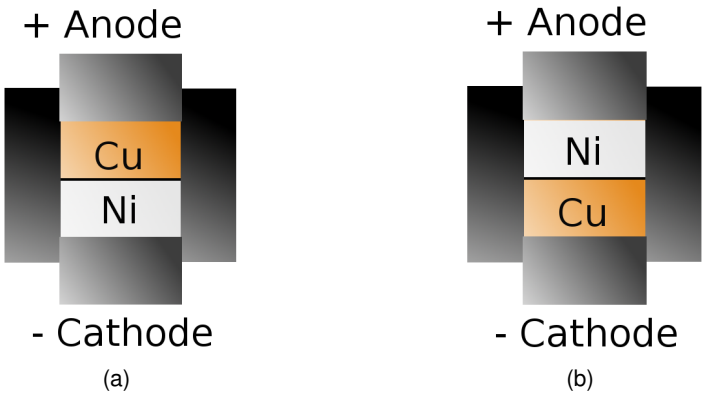

Figure 3.2: Copper and nickel pucks inside SPS die in the configuration (a) Cu/Ni; and (b) Ni/Cu.

Heating rates between 150^{o}C/min and 200^{o}C/min were used to attain the hold temperatures. Experiments were performed at hold temperatures of 750, 800, 850, 900, 950, and 1000^{o}C for a hold time of 1h, 2h, and 3h. A pressure of 50 MPa was used for these experiments. Additional experiments were done at 950^{o}C and 1000^{o}C for 3h with an applied pressure of 5 MPa. To produce control samples, a copper and nickel pair were placed in the SPS for a 5 min hold at the desired temperature to ensure bonding. These samples were then placed in a horizontal insertion vacuum furnace, shown in Figure 3.3, for the same times and temperatures as experiments conducted in SPS.

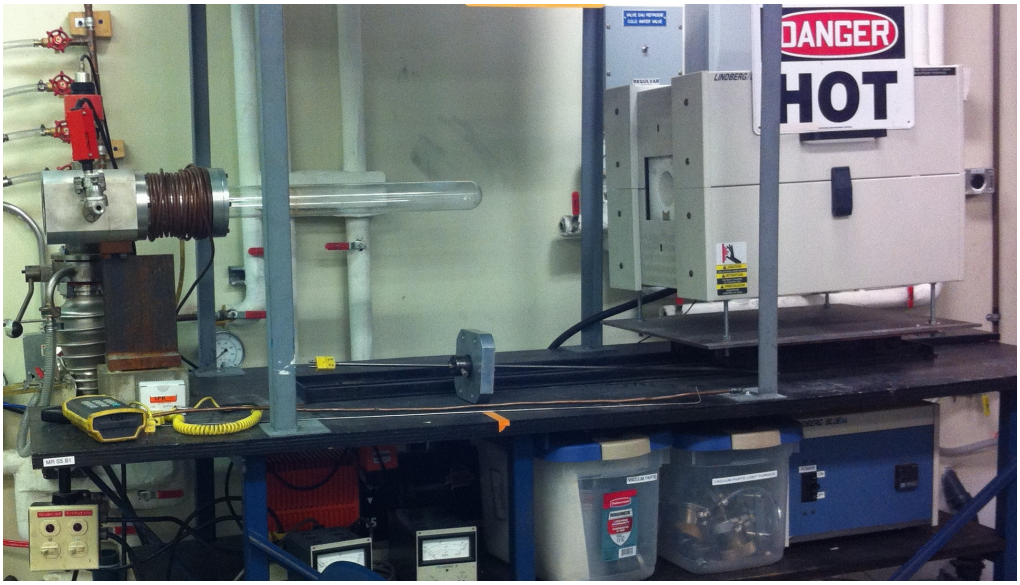

Figure 3.3: Horizontal vacuum furnace used for control experiments.

3.2.2 3D Experiments

Spherical -100+325 mesh 99.9% pure copper powder and 99.8% pure nickel powder were obtained from Alpha Aesar. A mixture of these powders was performed to generate a powder of 95 wt% Ni and 5 wt% Cu, denoted Ni5%Cu. A micrograph of the powder obtained by scanning electron microscopy (SEM) is depicted in Figure 3.4.

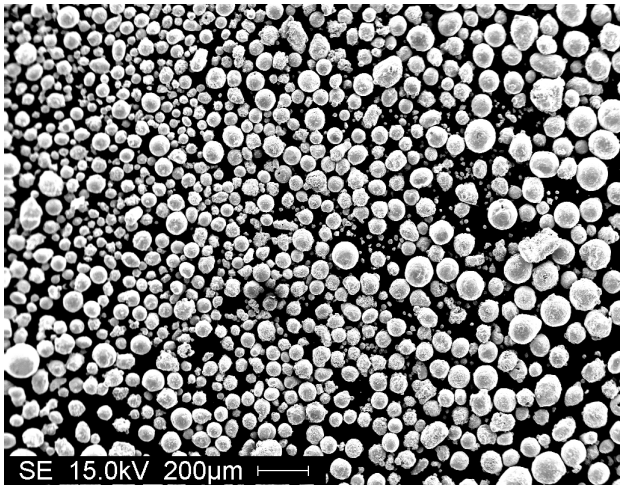

Figure 3.4: SEM micrograph of starting powder.

To obtain pucks of 20 mm in diameter and 5 mm in width, 33.55 g of the Ni5%Cu powder was put inside an SPS press. Runs of 30 min were performed at 700^{o}C, 800^{o}C, and 900^{o}C.

3.3 Spark Plasma Sintering Apparatus

A Thermal-Technology LLC 10-3 spark plasma sintering press, shown in Figure 3.5, was used.

Figure 3.5: Thermal-Technology SPS press.

It is comprised of a vacuum chamber, a hydraulic pump, a D.C. power supply, and a control system. The device is water cooled and argon gas is used to relieve the vacuum in the chamber for sample insertion and removal. Inside the vacuum chamber, the specimen is held inside a graphite die between two graphite punches as shown in Figure 3.6.

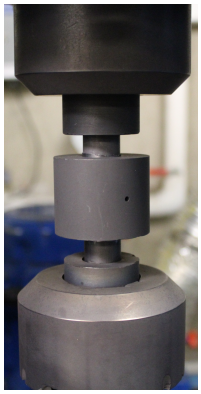

Figure 3.6: Punch and die set up inside vacuum chamber of SPS.

The temperature and time at which experiments are performed are adjusted by the control system. The amount of current used is dictated by the amount required to reach the specified temperature.

3.4 Chemical Analysis and Data Processing

All specimens generated by the SPS and vacuum furnace were sectioned along the diameter using a Buehler Isomet low speed saw with a diamond blade. The cross-sections were ground using 320, 600, and 800 grit grinding paper and then polished with 9 μm, 6 μm, and 1 μm monocrystalline diamond suspension. A final polish was performed using a Buehler Vibromet 2 vibratory polisher and a coloidal silica solution.

A Philips XL30 FEG-SEM scanning electron microscope was used for chemical analysis of the 1D diffusion couples. Backscattering electron (BSE) imaging was used to find the interface at the center of each sample. Energy-dispersive spectroscopy (EDS) was used for quantitative chemical analysis. An EDS line scan of 100 μm was taken across the interface of each sample. The dwell time per pixel was 6000 μs and each line scan contained approximately 800 points. An appropriate spot size was used to ensure that the dead time was between 20 and 40% and a working distance

of 10 mm was used to ensure an optimal amount of counts. Scans were performed at a voltage of 30 keV and BSE micrographs of the interface were taken for each specimen.

In order to obtain the weight percentages for each element, the Horny and Gauvin method was used [71]. First, a value, f, was calculated as the ratio of the intensity of one element over the total intensity.

$$f_{\text{Cu}} = \frac{I_{\text{Cu}}}{I_{\text{Cu}} + I_{\text{Ni}}} \tag{3.1}$$

Then a Monte Carlo simulation was performed to obtain a correction factor in order to calculate the appropriate weight fractions for each specific f value. This method ensures the removal of any discrepancies attributed to fluorescence or absorption. The f values were fitted to this correction using the following polynomial.

$$y = 0.006957f^6 - 0.02f^5 + 0.01533f^4 + 0.03423f^3 - 0.234f^2 + 1.1975f \tag{3.2}$$

Here, y is the weight fraction of the corresponding f value. Applying Equation 3.2 to f values across each line scan generated curves of weight percentages of copper as a function of distance. This fitting curve is unique to the quantification of copper in nickel.

A sigmoid function was fitted to each concentration curve in order to eliminate noise generated by the EDS scans. These fits were then used to calculate diffusion coefficients as a function of concentration. Diffusivities were calculated using the Sauer-Freise den Broeder method [9]. The following equation was used to obtain diffusion coefficients.

$$D(C') = \frac{1}{2t\left(\frac{dC}{dx}\right)_{x'}}[(1-\psi)\int_{x'}^{\infty}(C'-C_R)dx + \psi\int_{-\infty}^{x'}(C_L-C')dx] \tag{3.3}$$

In this expression, t is the annealing time, C_L is the concentration at the at the minimum distance, C_R is the concentration at the maximum distance, C' is the concentration at which D is calculated, x' is the corresponding distance, and $\psi = \frac{C'-C_R}{C_L-C_R}$. Diffusion coefficients were calculated for concentrations between 10 and 90 wt% Cu given that, outside these bounds, this method produces some significant amount of error. These diffusion coefficients were then used to calculate activation en-

ergies for both orientations and the control experiments. Activation energies were calculated at 60, 70, and 80 wt% Cu because these concentrations gave the most accurate linear fits. They were obtained by the slope, $-Q/R$, of the plot $\log(D)$ vs $1/T$.

Analysis of the sintered powder cross-sections was performed using a Hitachi SU-3500 FEG-SEM. Using BSE, copper particles were found within the nickel matrix. EDS was then used to obtain a compositional map of the area. A beam energy of 30 keV and beam current of 100 μA was used. Using AZtec data analysis software, quantitative element maps were obtained where the intensity of copper at each pixel was determined. The f-ratio was calculated using the intensities of both elements and the Horny and Gauvin method was subsequently used, as above, to obtain the corrected weight fractions [71].

4 The Effects of Applied Current on 1D Interdiffusion between Copper and Nickel in Spark Plasma Sintering

S. Rudinsky, R. Gauvin, and M. Brochu

4.1 Preface

A total assessment of the diffusion kinetics in SPS was performed by first studying diffusion in 1D and expanding to 3D to investigate diffusion of blended powders. The diffusion of copper, in the following work, was analyzed in the orientation parallel to the applied current. This was done through the use of bulk diffusion couples generated both in SPS and in a heating element furnace.

Abstract

Spark plasma sintering (SPS) is a powder metallurgy technique that employs the use of fast sintering kinetics to produce final consolidated components in a matter of minutes. In order to use blended powders in SPS to obtain fully alloyed parts, diffusion during sintering must be understood. An investigation into the effects of current on the diffusion of copper and nickel was performed using SPS. Bulk specimens were used to generate diffusion couples in SPS, in alternating orientations with respect to the direction of the current. Control samples were produced using a horizontal insertion vacuum furnace. Experiments were performed at temperatures between 850^{o}C and 1000^{o}C for 3h. Concentration profiles were obtained by scanning electron microscopy (SEM). Diffusion coefficients and activation energies were calculated for the SPS and samples annealed without current. It was shown that, at temperatures near $0.9T_m$, the application of current in SPS inhibits diffusion between copper and nickel due to the re-orientation of electrons caused by the loss of ferromagnetism in nickel. Activation energy for diffusion is, however, decreased due to the temperature gradients arising from the difference in resistivity between the two species.

4.2 Introduction

Spark plasma sintering (SPS) is a sintering process that has received a lot of attention over the past 5-10 years, compared to conventional sintering, as it allows the retention of unique microstructures and properties such as the retention of nanocrystalline structures [72, 73] and high yield strengths and bending strengths [74]. Similar to hot pressing, the powder consolidation occurs through a combined application of uniaxial pressure and heat. However, in SPS, the heat is generated through joule heating induced from a pulsed direct current passing through the powder bed and die assembly. Consequently, high heating rates can be obtained which promote bulk and grain boundary diffusion, and in turn decrease required sintering time significantly [3, 21, 75]. Typically, for metal, pre-alloyed powders are used in SPS which are associated with a higher cost feedstock than powder blends. Powder blends are a mix of the primary material and the alloying element particles. In order to obtain a fully alloyed final product with maximized isotropic properties, a homogeneous distribution must be obtained. While hot-pressing can produce a full distribution of elements, the typical duration for sintering is within hours. SPS can produce fully dense and fully sintered components in a matter of minutes. Consequently, shorter diffusion times can be used to attain homogeneity. To this date, diffusion kinetics in SPS are not well understood and it is unclear whether the existing diffusion kinetics are altered due to the presence of the applied current.

To provide insight on the role of electromigration on binary interfacial diffusion in the 1D case, Zhao et al. studied Cu-Ni diffusion couples with and without an applied current [76]. Their experimental set-up consisted of an apparatus that isolated temperature from the D.C. current and did not apply pressure [76]. Using the Sauer-Freise den Broeder method to calculate diffusion coefficients [9] and subsequent activation energies, they showed that the effective activation energy of diffusion in copper and nickel thin foils decreases by up to 50% at high Cu concentrations when a current density of 800 A/cm^2 is passed through the materials [76]. Other studies of the effects of pulsed D.C. on copper involve experiments on interconnects and wires to determine the mean time to failure (MTTF) due to electromigration [50, 77]. These authors have shown that the MTTF during constant applied current of copper wires due to the presence of electromigration is shorter then the MTTF when a pulse current is used. Experiments on the effects of current on atomic movement in

copper have been performed repeatedly with conventional circuitry [38, 42, 53, 78] however none exist using spark plasma sintering.

The current work tackles the discrimination of the effect of the electric field through performing diffusion couple experiments using copper and nickel in an SPS apparatus. This work desires to establish the understanding of the diffusional relationships under the influence of an electric field in a one-dimensional (1D) binary configuration. The Cu-Ni system is a model system for diffusion studies because the two elements form a complete solid solution and diffuse through vacancies [10]. It is, therefore, a widely studied system. The role played by the electric field on diffusion was observed through chemical profiles, changes in diffusivities, and their respective activation energies.

4.3 Experimental Procedure

Copper (99.99%) and nickel (99%) rods 20 mm in diameter were used and pucks of 5 mm in thickness were extracted. The mating surfaces were polished down to 1 μm using diamond paste and rinsed in water and acetone to remove all remaining traces from the polishing steps. The diffusion couples were performed in a Thermal Technology 10-3 SPS press at temperatures of 850, 900, 950 and 1000^{o}C for a holding time of 3 hours. Two configurations were studied, namely Cu/Ni and Ni/Cu, to evaluate if diffusion directionality, depending on the orientation of the applied current, is occurring. Cu/Ni is used as a convention to indicate that the current is passing from copper to nickel. As control experiments, diffusion couples were initially joined in the SPS at the desired diffusion temperature for 5 minutes, only to ensure proper inter-facial bonding. Thereafter, the samples were annealed at the corresponding test temperature in a heating element furnace to obtain solely thermally activated diffusion.

The diffusion couples were cross sectioned along the diameter, followed by hot mounting and standard metallographic procedures down to colloidal silica (0.05 μm). The quantitative chemical composition profiles were obtained through energy dispersive spectroscopy (EDS) line scan analysis using a Philips XL-30 scanning electron microscope (SEM). The interface was found using backscattered electron imaging (BSE). Line scans of 100 microns in length were taken across the

interface. Figure 4.1 shows a representation interface over which the analysis was done.

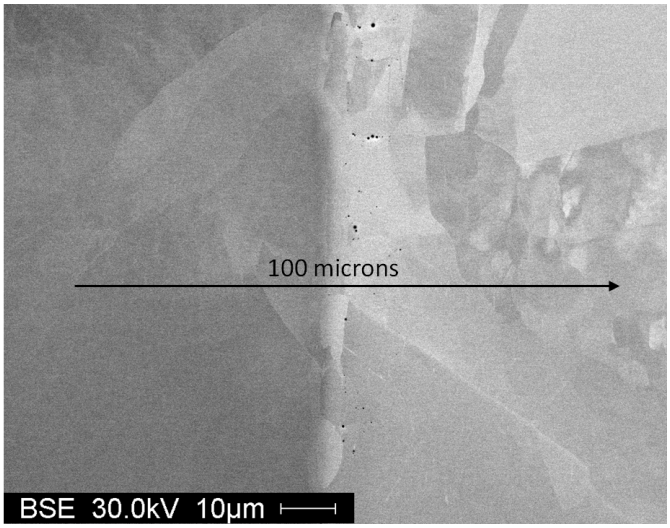

Figure 4.1: BSE micrograph of cross-section showing position of line scan.

The relative intensity of copper was measured and, using a correction curve generated by a Monte Carlo simulation, the appropriate weight fractions were obtained [71]. A sigmoid curve was fitted to each concentration curve in order to reduce discrepancies attributed to EDS noise. Each sigmoid curve had a coefficient of determination $R^2 = 0.99$. Diffusion coefficients were then calculated using the Sauer-Freise-den Broeder (SFB) method, which generated concentration dependent diffusion coefficients through the following equation:

$$D(C') = \frac{1}{2t\left(\frac{dC}{dx}\right)_{x'}}[(1-\psi)\int_{x'}^{\infty}(C'-C_R)dx + \psi\int_{-\infty}^{x'}(C_L-C')dx] \tag{4.1}$$

where $\psi = \frac{C'-C_R}{C_L-C_R}$, C' is the concentration at which the diffusion coefficient is to be calculated, and C_L and C_R are the concentrations at the extremities [9]. This method produces some significant calculation error for concentrations below 10 wt% and above 90 wt%, as reported by Glicksman [10]. Therefore, diffusivities were calculated for concentrations between these two bounds. To obtain the effective activation energies of diffusion, the Arrhenius approach was used to analyze the expression,

$$D = D_0 e^{(-Q/RT)} \tag{4.2}$$

where Q is the activation energy, T is the absolute temperature, R is the gas constant, and D_0 is

the pre-exponential. The activation energy was extracted from the slope of the linear plot $\log(D)$ vs $1/T$.

4.4 Results

Figures 4.2(a)-(d) show the concentration curves of the Cu/Ni, Ni/Cu, and furnace diffusion couples at 850, 900, 950, and 1000^{o}C, respectively. These curves are plotted within the valid limits of the SFB method.

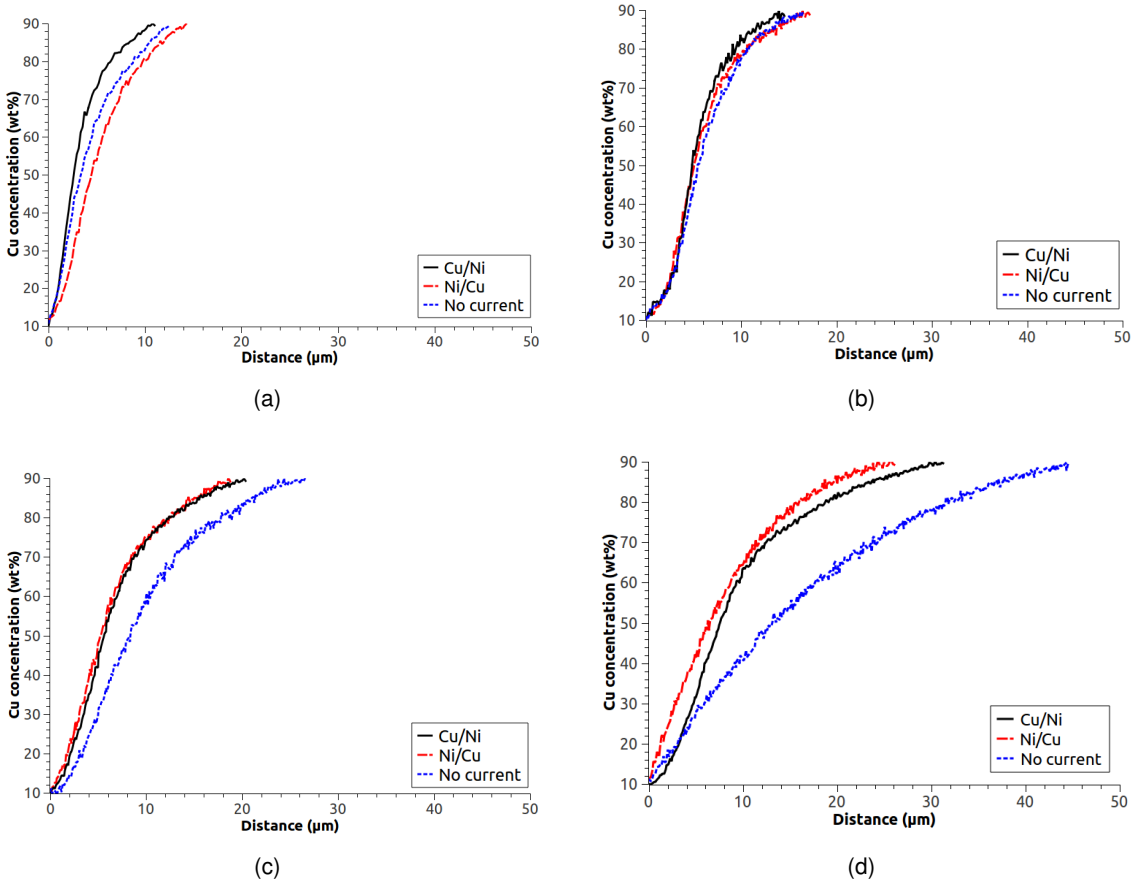

Figure 4.2: Concentration profiles of diffusion couples heated for 3h at (a) 850^{o}C; (b) 900^{o}C; (c) 950^{o}C; and, (d) 1000^{o}C.

At 850^{o}C and 900^{o}C, all curves overlap and span across the same distance suggesting that there is no difference in interdiffusion between SPS, regardless of orientation, and annealing without current. At 950^{o}C, both the concentration profiles of the samples produced in SPS still overlap, showing similar diffusion progression. However, the sample annealed without current shows a longer diffu-

sion profile, which indicates that the interdiffusion has progressed further than the SPS samples. At 1000^{o}C, the difference between the diffusion distances and curvatures is greater and much more noticeable. The sample annealed without current shows an appreciable increase in diffusion distance. In all, Figure 4.2 shows that at higher temperatures, interdiffusion between copper and nickel is inhibited in SPS compared to annealing without current.

Diffusion coefficients were calculated from the sigmoid fits of each concentration curve. The results of the obtained diffusion coefficients at 850^{o}C and 1000^{o}C are shown in Figure 4.3.

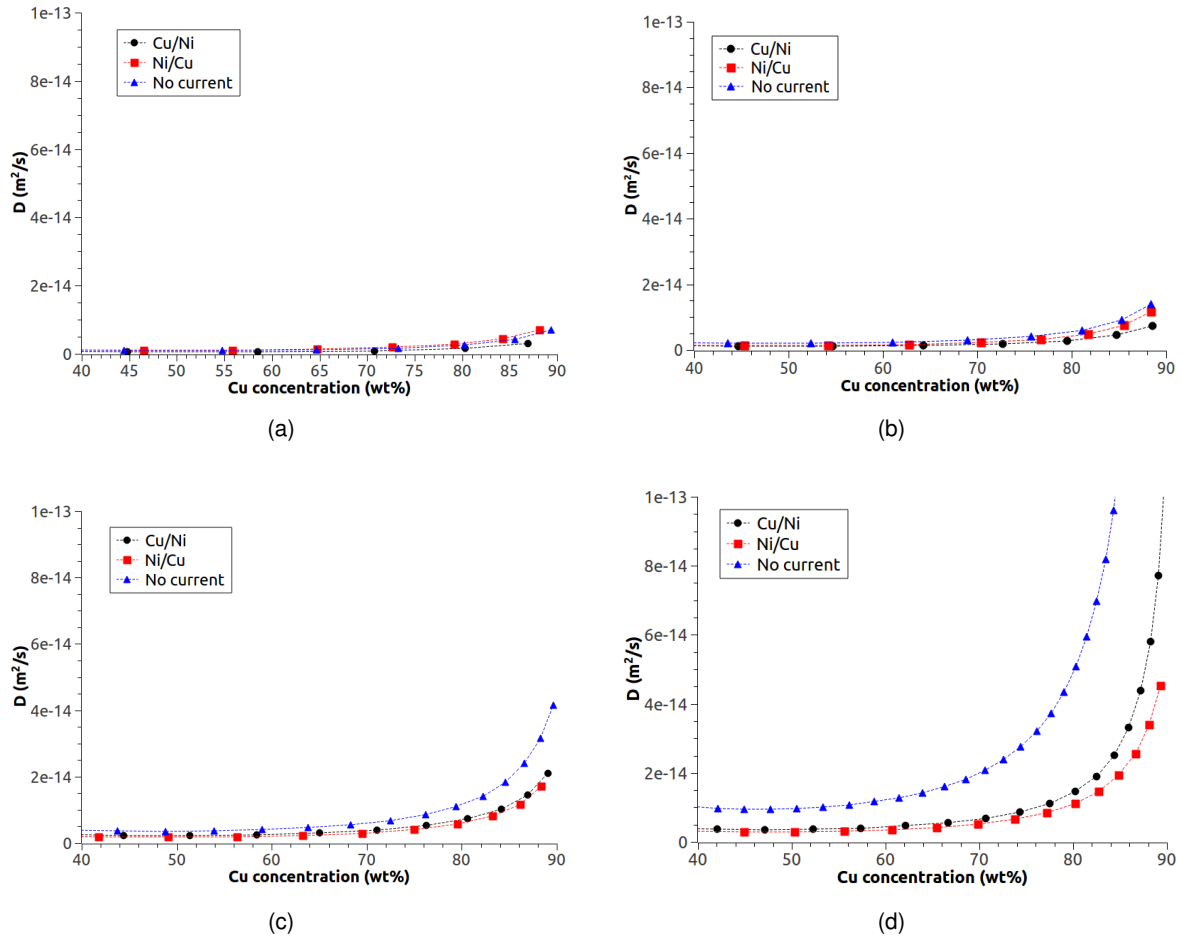

Figure 4.3: Diffusion coefficients of diffusion couples heated for 3h at (a) 850^{o}C; (b) 900^{o}C; (c) 950^{o}C; and, (d) 1000^{o}C.

It is seen that while at 850^{o}C the diffusion coefficients of all three experiments are within the same order of magnitude, at 1000^{o}C the diffusion coefficients of the sample annealed without current are

constantly an order of magnitude higher than those in SPS, indicating that these diffusion coefficients are greatly increased. The diffusion coefficients of the sample annealed without current are in agreement with literature values. Tronsdal *et al.* reported that, at 1000^{o}C, the diffusion coefficient of copper in nickel is 3.3×10^{-14} m^2/s at 60 wt% Cu [79], which fits the present work's data $D = 1.28 \times 10^{-14}$ m^2/s. Comparisons were also made with Anusavice *et al.* [67] and Monma *et al.* [66]. A comparison between the present work and their results is shown in Figure 4.4.

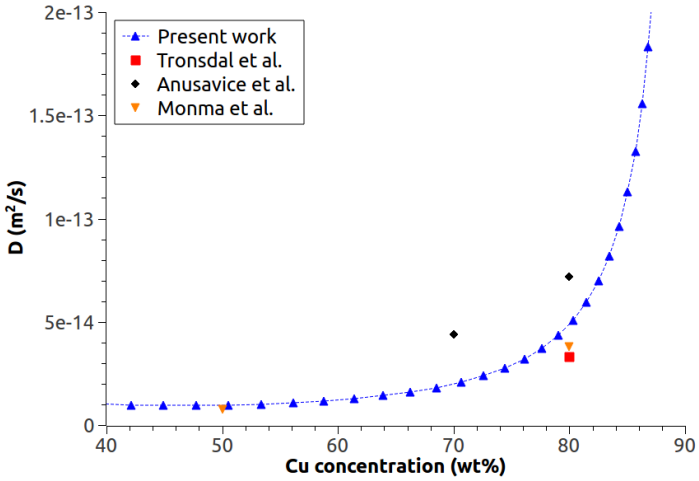

Figure 4.4: Comparison of diffusion coefficients at 1000^{o}C between the present work and existing literature.

Activation energies were calculated for all experiments performed. Because activation energy is a function of the diffusion coefficient and the SFB method produces concentration dependent diffusion coefficients, activation energies were calculated at various weight percentages of copper. Plots of $\log(D)$ vs $1/T$ were generated and a linear fit was performed to obtain the slope, as shown in Figure 4.5 for 60 wt% Cu.

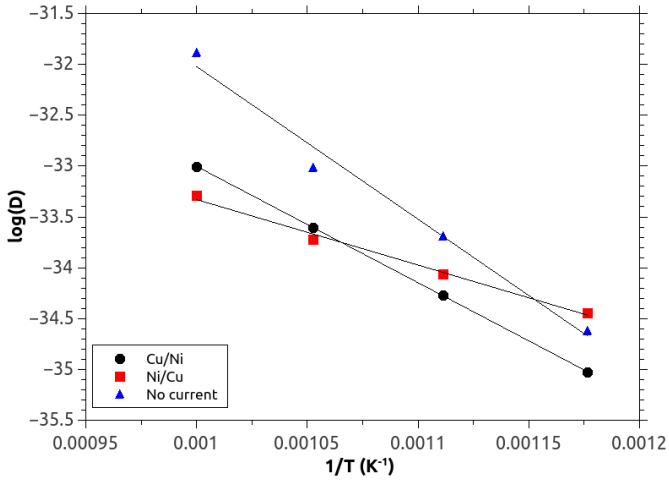

Figure 4.5: Linear fit of all samples at 60 wt% Cu.

Activation energies were calculated at 60, 70, and 80 wt% Cu because these generated the most reliable linear fits. The results are shown in Tables 4.1(a)-(c).

Table 4.1: Activation energies for diffusion at (a) 60 wt% Cu; (b) 70 wt% Cu; and (c) 80 wt% Cu.

(a)

wt%	Q (kJ/mol)	R^2
Cu/Ni	160	0.99
Ni/Cu	90	0.99
No current	211	0.99

(b)

wt%	Q (kJ/mol)	R^2
Cu/Ni	164	0.99
Ni/Cu	85	0.94
No current	208	0.96

(c)

wt%	Q (kJ/mol)	R^2
Cu/Ni	182	0.99
Ni/Cu	109	0.99
No current	221	0.99

The SPS samples show lower activation energies than annealing without current with the lowest seen for the Ni/Cu orientation. Zhao *et al.* had also observed a decrease in activation energy of diffusion with the application of current compared to diffusion couples produced without applying current [76]. The results obtained for thermal diffusion are near accordance with literature values which stipulate that the activation energy for diffusion of copper into nickel is 218$\pm$2 kJ/mol at 70 wt% Cu and 215$\pm$3 kJ/mol at 80 wt% Cu [67].

4.5 Discussion

4.5.1 Existence of electromigration

A well-known consequence of applying a direct current to a metal is electromigration [47–50]. The electron wind generated by the current applies a force on the atoms of the conductive substance through collisions between these electrons and the atomic nuclei [43]. As a result, atoms upstream from vacancies are encouraged to migrate and will forcefully occupy said vacancies [43]. This force counters that of the electric field which causes the positively charged nuclei to migrate opposite the flow of electrons. Consequently, atoms travel with ease in the direction of the electron flow and the vacancies travel more readily in the opposite direction [43]. The atomic drift velocity attributed to electromigration is described by Equation 4.3.

$$v_{em} = \left(\frac{D}{kT}\right) eZ^* \rho j \exp\left(\frac{-Q}{kT}\right) \tag{4.3}$$

Here, D is the diffusion coefficient, k is Boltzmann's constant, T is the annealing temperature in Kelvin, eZ^* is known as the "effective change" of the material and is the product of the electronic charge and the effective charge of the material, ρ is the resistance, j is the current density, and Q is the activation energy for atom movement in J [49]. Consider diffusion of copper occurring at 1000^{o}C where the interdiffusion coefficient is $D = 5.1 \times 10^{-14}$ m^2/s at 80 et% Cu and, in SPS, the current density is 300 A/cm^2. For copper, the effective charge is -14 [52] and its resistivity at 1000^{o}C is $9.35 \times 10^{-8}\Omega$m [80]. Therefore, from Equation 4.3, the drift velocity due to electromigration in SPS at the specified temperature is 2.75×10^{-21} m/s. Such velocity can be considered negligible in the overall atomic movement. The primary explanation arises from the current density, j, whose variation substantially affects the magnitude of the electromigration effect on atomic velocity. Now, in order to perceive noticeable effects of electromigration in a material, current densities of at least $10^3 - 10^5$ A/cm^2 must be used [42]. Therefore, the current densities used in SPS are just below the window to induce electromigration.

4.5.2 Effect of the loss of ferromagnetism in nickel

At the high temperatures of 950 and 1000^{o}C, Figures 4.2(c) and 4.2(d) show that diffusion distance in SPS is lowered. This can be explained by the combination of the change in the electron band structure of nickel during heating and the electric field. Nickel's ferromagnetic properties arise from the electron configuration in the 3d-like band. While for copper the d band is full, in nickel the number of electrons in the d band is non-integral, i.e. that there are missing states or holes in the band [81]. This causes a degeneration of energy of one spin orientation compared to the other [82]. As a result, there are two Fermi surfaces for each spin and the density of states is not symmetric for both orientations [82].

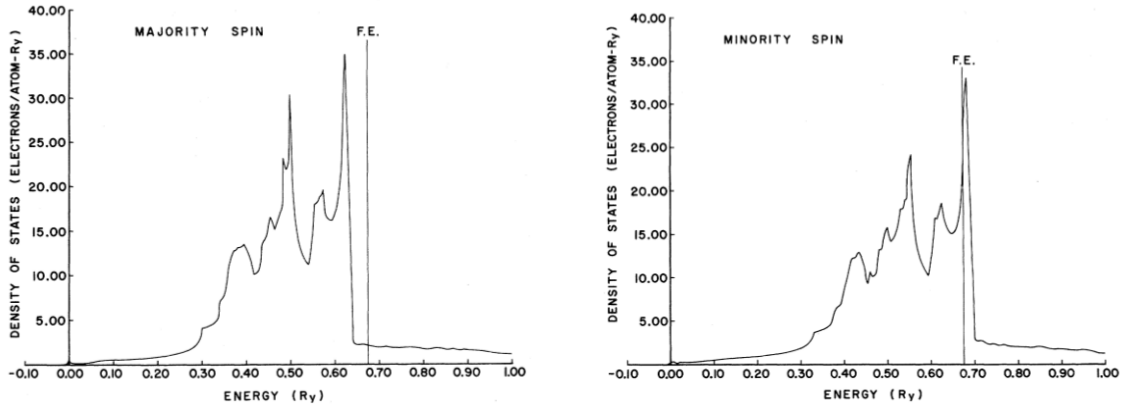

(a) (b)

Figure 4.6: Density of states of Ni for (a) majority (up) spin and (b) minority (down) spin [82].

Figures 4.6(a) and 4.6(b) show the lack of spin up electrons in high energy states compared to spin down in nickel. In non-ferromagnetic metals, the density of states for both spins resembles that of Figure 4.6(b) [83].

Now, as temperature increases, the loss of nickel ferromagnetism is due to the appearance of spin waves [84–86]. Spin waves are propagating disturbances in the ordering of a magnetic material. Like phonons, spin waves can be treated as particles but they are vibrational artifacts [87]. There is a high excitation of these spin waves at high temperatures and this causes re-ordering of the electrons in the nickel band structure [87]. Therefore, changes in spin and position of electrons in the d and s bands must occur in order to generate this single Fermi level in nickel at high temperatures.

Once the band structure of nickel is symmetric for both spins, it can be considered that nickel takes on a different electron configuration [88]. To summarize, at high temperatures, the order of the band structure in nickel is altered due to vibrational artifacts known as spin waves and the electrons are distributed in a different manner compared to nickel in its original ferromagnetic state.

The previous discussion only takes into account the properties of pure Ni. Now, consider the addition of small concentrations of copper in the nickel matrix. It is important to note that the d level of nickel is of higher energy than that of copper [89]. Due to this property, when a nickel atom is placed within a copper matrix, the difference in energies causes a local repulsive potential with respect to the d band. With increasing nickel content, this causes the occurrence of local clustering which, while creating a repulsive potential, also resists heat increase [90–92]. These clusters are on the order of 12-13 atoms which create short-range disorder in the lattice [93, 94]. Now, consider the addition of an applied current to the described system. Even though SPS uses a pulsed D.C., the pulses are rapid enough to allow the treatment of this situation as being subjected to a constant flux of electrons. The constant presence of electrons through the diffusion couple caused by the application of current implies that the conduction band between the copper and nickel nuclei contains a surplus of electrons. Due to exchange interactions in ferromagnetic materials, electrons in close proximity to nickel atoms will tend to be aligned similarly [95]. As temperature is increased and there is re-arrangement of electrons in the band structure causing the loss of ferromagnetism, the repulsion of the d bands between species is greatly enhanced with the excess of the similarly aligned electrons arising from the influx of current. This causes a repulsive chemical potential in the system which reduces the diffusing velocities of the species by inhibiting a copper atom from occupying a vacancy in close proximity to the nickel clusters. Consequently, the diffusion distance of copper in SPS is reduced. A schematic is shown in Figure 4.7.

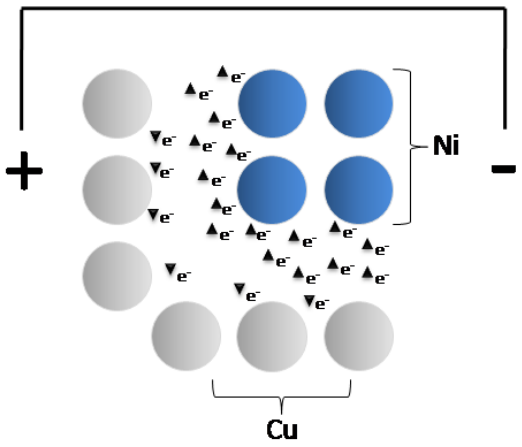

Figure 4.7: Schematic of repulsive potential causes by orientation of electrons.

Given that this is a repercussion of the presence of an electric current, directionality is not a contributing factor. The resulting effect, as shown in Figure 4.3, is the decrease of the diffusion coefficient of Cu in SPS. This value is reduced by an order of magnitude which demonstrates the significance of the increased hindering of diffusion caused by the repulsive force. In all, although re-arrangement of the band structure occurs in nickel without the presence of an applied current, the surplus of electrons, which are encouraged to orient themselves similarly to the d-band electrons of nickel, are responsible for enhancing the repulsive chemical potential to a significant and noticeable level.

4.5.3 Effect of SPS on activation energy

There is, however, a decrease in activation energy seen in SPS. Because activation energy is independent of temperature, any effects which are dependent on temperature such as the chemical potential repulsion seen at $0.9T_m$ are unrelated to activation energy. However, activation energy can change if there exist temperature gradients within the system [96]. Given that nickel's resistivity is higher than copper, as current is being applied, nickel will increase in temperature much more rapidly then copper [5]. This is especially true when the current is first passing through nickel. This creates a temperature gradient from nickel to copper which decreases the energy required in order to induce diffusion. Therefore, even though at high temperatures diffusion is inhibited by atomistic effects, the activation energy for diffusion is lowered facilitating the initiation of the process.

4.6 Conclusion

Diffusion couple experiments were performed using spark plasma sintering. These experiments were compared to conventional diffusion performed in a vacuum furnace. Concentration profiles were generated and diffusion coefficients and activation energies were calculated for all processes. This study has shown that near $0.9T_m$ diffusion is inhibited in SPS. This is caused by the re-orientation of electrons during the loss of ferromagnetism in nickel. This phenomenon causes a negative chemical potential between the two species. Activation energy for diffusion was shown to be decreased in SPS compared to conventional diffusion which is a result of the high temperature gradients caused by the difference in resistivity between the two species.

5 Interdiffusion between Copper and Nickel Powders during Spark Plasma Sintering

S. Rudinsky and M. Brochu

5.1 Preface

The previous chapter reported diffusion in SPS in 1D, parallel to the applied current. This chapter assesses diffusion in 3D with the 1D work as a starting block. This was performed through the use of blended copper and nickel powders.

Abstract

An investigation into sintering blended powders by spark plasma sintering (SPS) was performed using a powder blend composed of 5 wt% Cu and the remaining portion nickel. Pucks were sintered at 700, 800, and 900^{o}C for 30 minutes. Isolated copper particles were analyzed by energy-dispersive spectroscopy (EDS) and compositional maps were obtained of the area surrounding the particle. It was shown that diffusion at such temperatures is uniform parallel and perpendicular to the applied current. Diffusion coefficients were calculated and it was shown that these values are similar perpendicular and parallel to the applied current. Activation energies for diffusion were obtained and demonstrated that diffusion within a powder is facilitated compared to bulk samples due to the geometry. Through two solutions to the diffusion equation, the sintering time to obtain a uniform distribution of 10 wt% Cu was calculated at all temperatures. It was ascertained that, below $0.8T_m$, there is no preferential direction for diffusion in SPS. However, the sintering time required to obtain a component containing a uniform distribution of copper surpasses that of conventional methods.

5.2 Introduction

Spark plasma sintering (SPS) has been researched as an alternative sintering method to conventional powder metallurgy techniques. Due to the generation of high heating rates and the application of pressure during the process, components can be produced within minutes [3]. SPS is often compared to hot pressing in that both apply pressure during heating. However, characteristic sintering times required for hot pressing are on the order of a few hours [1]. In SPS, a pulsed D.C. is applied across a specimen contained inside a conductive die between two punches. While the punches apply pressure to the powder, the current induces joule heating at the particle contacts. This heat surge promotes grain boundary and bulk diffusion and allows for rapid consolidation of the powder [3, 21, 75]. Typically, pre-alloyed powders are sintered in SPS; however, powder blends provide a cheaper alternative as there is no need for alloying prior to consolidation. In order to obtain a fully alloyed final product, the elements of a blend must diffuse uniformly so as to ensure a proper alloy distribution throughout the component. Given that SPS employs rapid sintering mechanisms, the existing diffusion kinetics must be understood in order to maximize the effectiveness of the process.

Few studies have been performed on sintering powder blends in SPS. Investigations into sintering TiAl powder blends were performed by Sun *et al.* using SPS by employing a 2-step annealing program [97]. The goal of the study was to obtain a nanostructured product composed of the γ-TiAl phase. Cryo-milling was performed prior to consolidation and the annealing process was in the form of reactive sintering. The effect of current on phase transformations and microstructure was studied while the current effect on atomic movement was not addressed [97]. Sintering of blended powders in SPS was also performed by Murakami *et al.* [98]. Using a Nb-AlN powder blend, it was determined that, due to short sintering times employed by SPS, the microstructure obtained after sintering was inhomogeneous throughout the compact [98]. Again, the focus of the study was on the final phases and microstructure obtained and not on the diffusion kinetics themselves. Even though sintering powder blends with SPS has been somewhat performed previously, the relation between diffusion kinetics and the processing parameters are still not well understood and as a result inhomogeneous microstructures and partial diffusion-based phase transformations are obtained.

In this study, the effect of current on a blend of copper and nickel powders is investigated. Given that these elements form a complete solid solution and diffuse through vacancies, they are a model system for experimentation on diffusion and are therefore the ideal candidates for a study on diffusion kinetics in SPS. A blend consisting of 5% copper was used in order to observe the diffusion of a single copper particle in a nickel matrix. Experiments were performed at a variety of temperatures within the limits of typical sintering and concentration maps, diffusion coefficients, and activation energies were obtained to investigate the diffusion progression during sintering. The time to obtain full homogeneity was subsequently calculated using solutions to the diffusion equation.

5.3 Experimental Procedure

Spherical -100+325 mesh 99.9% pure copper powder and 99.8% pure nickel powder were blended to obtain a powder mix of 5 wt% Cu and 95 wt% Ni. Using a thermal-technology 10-3 SPS press, the powder blend was sintered into 20 mm diameter pucks with a thickness of 5 mm. Experiments were performed at 700, 800, and 900^{o}C for 30 min. The pucks were then cross-sectioned and polished down to a 1 μm finish using standard metallographic procedures. A Hitachi SU3500 scanning electron microscope (SEM) was used for chemical analysis. Energy-dispersive spectroscopy (EDS) was used to obtain chemical composition maps of the area containing the copper particle. Intensities were obtained in terms of number of counts from the EDS detector and the Horny and Gauvin method was used to obtain corresponding weight fractions of copper [71]. This method employs the use of a Monte Carlo simulation of the electrons' interactions with the materials to obtain a correction curve. This curve is then applied to the relative intensities [71] to obtain the appropriate weight percentages. Weight percentages of copper were plotted as a 2D map to show the area where the copper had diffused. Diffusion coefficients were obtained parallel and perpendicular to the applied current, from low to high copper concentrations through the Sauer-Freise den Broeder method [9]. Activation energies were obtained by the Arrhenius plot of the diffusion coefficients. Finally, the time to obtain a fully homogenized component was calculated using two solutions to the diffusion equation: the homogenization model and the binary diffusion model.

5.4 Results and Discussion

5.4.1 Concentration Maps

Contour maps of copper concentrations at all conditions are shown in Figure 5.1.

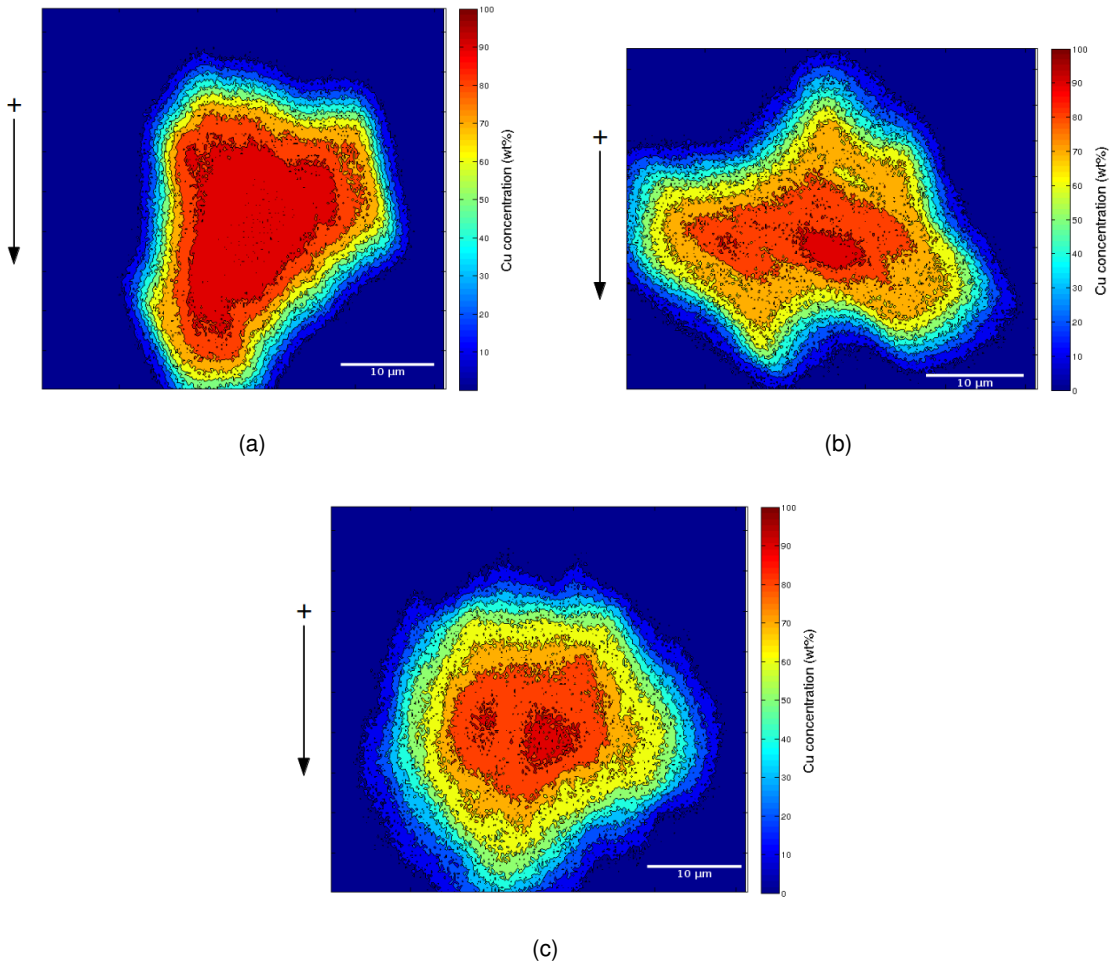

Figure 5.1: Copper concentration by area for compacts sintered for 30 min at (a) 700^{o}C; (b) 800^{o}C; and (c) 900^{o}C.

At 700^{o}C, the particle is mainly composed of near 100 wt% Cu with a small contour of diffusion about the core. With increasing temperature, areas of 60-70 wt% Cu are larger and the area through which copper has diffused is much greater. The center of the particle has a corresponding lower copper concentration. At 900^{o}C, diffusion from the center of the particle attains much further regions of the nickel matrix. The increase of diffusion area with temperature follows from the thermal activation property of diffusion [4]. In all conditions, diffusion is uniform about the center of the original copper

particle. There are no high diffusion paths in any specific direction suggesting that there is no directionality effect of the electric field.

5.4.2 Diffusion Coefficients and Activation Energy of Diffusion

Diffusion coefficients were calculated from the center of the copper particle outward in directions parallel and perpendicular to the current. The results are shown in Figure 5.2.

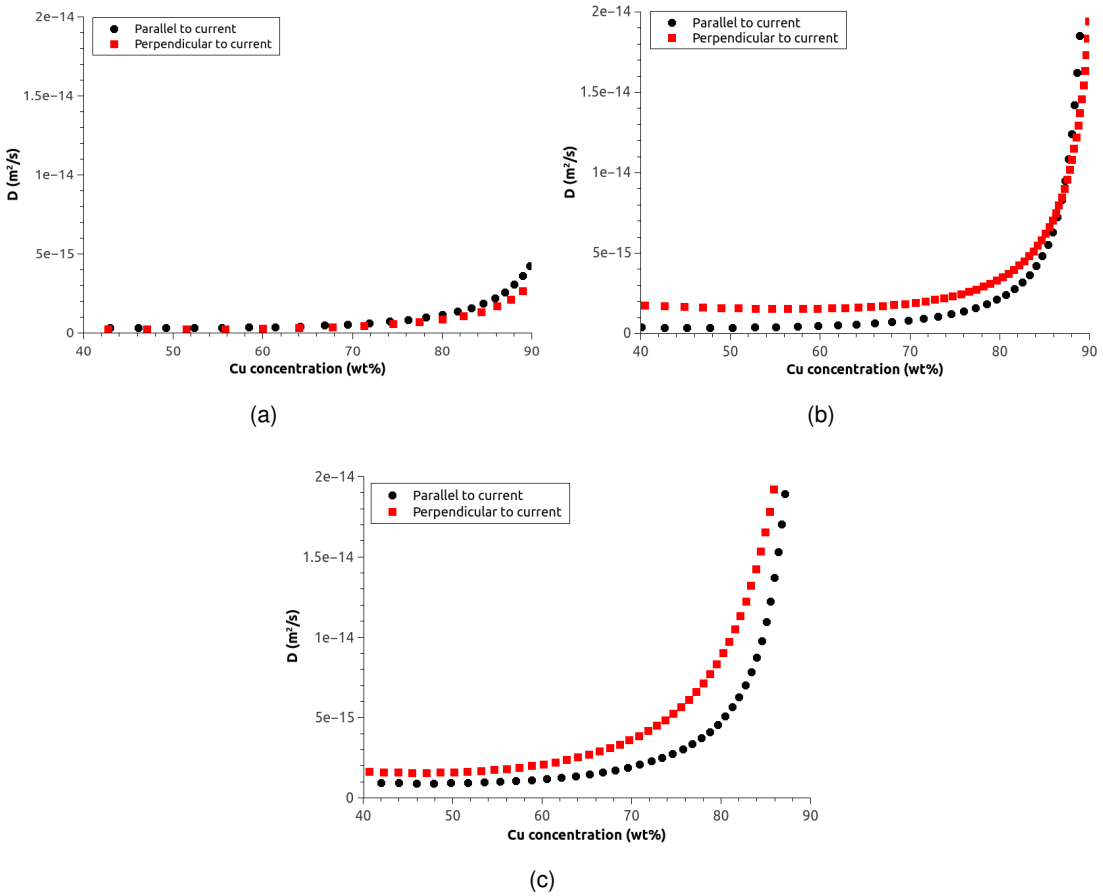

Figure 5.2: Diffusion coefficients parallel and perpendicular to applied current for experiments conducted at (a) 700^{o}C; (b); and (c) 900^{o}C.

In all conditions, diffusion coefficients parallel and perpendicular to the applied current are similar throughout the entire range of copper concentrations. A comparison between the diffusion coefficients of the powder blend and those obtained in the previous chapter is depicted in Figure 5.3.

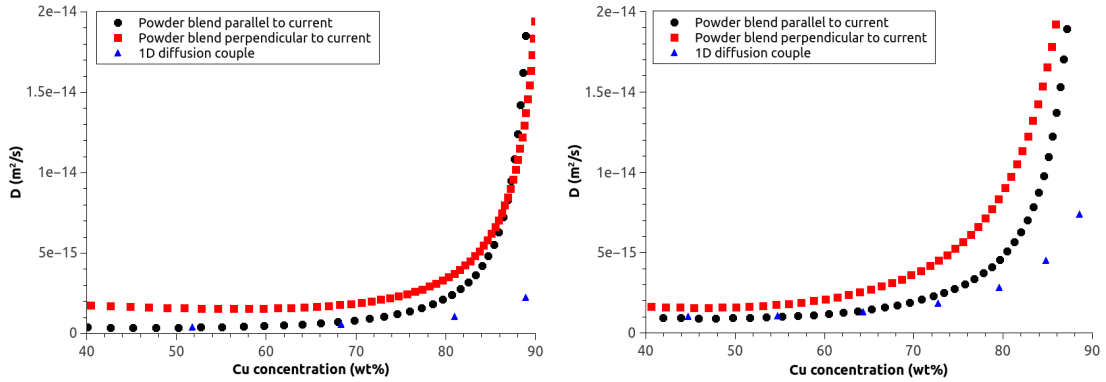

(a) (b)

Figure 5.3: Diffusion coefficients of powder blend compared to 1D bulk diffusion couple at (a) 800^{o}C and (b) 900^{o}C.

Diffusion coefficients obtained from the diffusing copper particles are similar to those obtained in the 1D bulk diffusion couple. There is, however, a slight increase in the diffusion coefficients of the powder blend at higher copper concentrations. This is due to the difference in geometry. Given that grain boundaries are formed at prior particle boundaries, the contribution of grain boundary diffusion to the effective diffusion coefficient is greater in a powder sample [1]. Also, penetration of a diffusing species through a spherical boundary is facilitated compared to a flat interface because destruction of the original interface, in the 1D case, requires a larger amount of energy. This is further seen by the obtained activation energies for diffusion of copper in the powder blend, displayed in Table 5.1.

Table 5.1: Activation energy for diffusion of copper into nickel in powder blend

wt% Cu	Q (kJ/mol)	R^2
60	56	0.94
70	58	0.94
80	70	0.99

The activation energies are lower in the sintered powder blend compared to the previous chapter, showing the additional diffusional and geometrical contributions.

When applying high currents during annealing, it was found that there is a preferential direction of diffusion parallel to the applied current caused by electromigration [76]. However, previous studies have determined that electromigration does not occur in SPS [31]. It was also shown in the

previous chapter that, parallel to the current, there is no difference in diffusion distance between SPS and annealing without current at temperatures lower than $0.8T_m$. Therefore, when sintering powder particles, the diffusion seen here occurs in an analogous fashion to hot pressing. Parallel to the current, there is no effect of directionality on diffusion in SPS and Figures 5.1 and 5.2 show that there is no directionality effect perpendicular to the current either. Studies performed using electric discharge sintering, a form of field-assisted sintering, showed necking occurred quicker parallel to the current than perpendicular [99, 100]. This sintering method uses high voltages and current densities on the order of 10^7 A/cm^2 in order to create a discharge that induces melting and particle wetting [99, 100]. On the other hand, current densities attained in SPS for temperatures used in this experiment are 250 A/cm^2 on average. Without the high current and high voltage conditions, there is no melting and mass transport occurs only through solid state diffusion [99].

5.4.3 Sintering Time for Full Homogeneity

The bounds of the SFB method do not permit the calculation of the amount of time required to obtain a uniform distribution of 5 wt%Cu through a component. However, an estimation can be made assuming the use of a powder blend of 10 wt%Cu. Two solutions to the diffusion equation are applied to calculate the sintering time required to obtain an SPS part containing a homogeneous distribution of copper. First, the infinite binary diffusion couple solution is used, shown in Equation 5.1.

$$t_{bin} = \left(\frac{x}{2\text{erf}^{-1}(1-C)} \right)^2 \times \frac{1}{D} \tag{5.1}$$

Here, x is half of the mean distance between particles, C is the desired uniform concentration, and D is the diffusion coefficient [4]. Subsequently, the homogenization solution to the diffusion equation is employed for the same temporal calculation. This is depicted in Equation 5.2,

$$t_{hom} = -\ln\left(\frac{C}{\sin(\frac{x\pi}{l})} \right) \times \tau \tag{5.2}$$

where l is the distance between subsequent particles and τ is the relaxation time calculated by the following expression [4].

$$\tau = \frac{l^2}{\pi D} \tag{5.3}$$

The results of both models are shown in Figure 5.4.

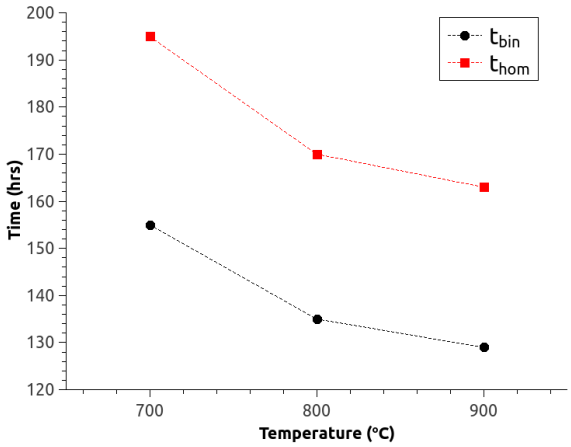

Figure 5.4: Sintering times to obtain 10 wt%Cu homogeneity in a component produced by SPS.

Throughout these calculations, D is fixed even though the change in concentration at the core of the particle brings about a change in the diffusion coefficient. However, results obtained using D at 50 wt% Cu, the point of minimal concentration gradient, are within the same order of magnitude as those obtained at 10 wt%Cu. Therefore, the assumption that D is fixed is an acceptable approximation due to the minor difference in resulting sintering times between high and low concentration gradient areas.

Figure 5.4 demonstrates that the two solutions to the diffusion equation produce sintering times required to obtain a uniform distribution of 10 wt%Cu that are on the order of 10^2 hours. This far exceeds typical sintering times used in hot pressing. Therefore, even though diffusion is uniform in SPS, the required sintering times to obtain a fully homogeneous component are not practical and surpass those of the equivalent conventional method.

5.5 Conclusion

A nickel and copper powder blend containing 5 wt% Cu was sintered by SPS. EDS analysis was performed on isolated copper particles in order to observe the diffusion of copper from the center of the particles outward. It was found that diffusion of copper occurs uniformly regardless of orientation with respect to the applied current. Diffusion coefficients were found to be similar whether diffusion

occurred perpendicular or parallel to the current. However, the sintering time required to produce a component containing a homogeneous distribution of copper far exceeds that which is typical of hot pressing. Sintering blended powders in SPS is, therefore, impractical if a fully alloyed component is desired.

6 Summary

- The Cu-Ni system was used to investigate diffusion in SPS in order to determine the role played by the applied current during sintering. The diffusion kinetics were studied in order to create the possibility of employing the use of powder blends in obtaining fully alloyed components by SPS.
- Diffusion in 1D was investigated using bulk copper and nickel. It was determined that diffusion is inhibited in SPS at temperatures near $0.9T_m$ compared to annealing without current. This occurred regardless of the direction of the applied current through the diffusion couple. Other studies had shown that, due to electromigration, diffusion is enhanced when nickel diffuses in the same direction as the electron flow [76, 77], however it was determined that current densities greater then those employed in SPS must be used in order to observe such effects [49]. The cause of reduction in diffusion in SPS compared to annealing without current is the existence of a repulsive chemical potential inhibiting atomic movement in the direction of the concentration gradient. This repulsion arises from the surplus of electrons in the conduction band during the application of current and the re-orientation of electrons in nickel's band structure as nickel loses its ferromagnetic properties [88]. When copper is introduced into the system, there is clustering of the nickel atoms [90] and the excess electrons undergo a tendency to orient themselves similarly to those in nickel's band structure [95] causing a repulsive force against the copper atoms surrounding the clusters. With surrounding vacancies, a copper atom is more likely to occupy vacancies further from the nickel cluster causing a decrease in the diffusion of copper into nickel.
- At lower temperatures, diffusion distances were the same in all cases suggesting that this effect does not occur at such temperatures. These low temperatures are still above the lower limit of typical sintering temperatures, i.e. above $0.6T_m$, and it can, therefore, be asserted that diffusion

in SPS can resemble conventional sintering at the lower end of sintering temperatures.

- The activation energy for diffusion was found to be lower in SPS indicating that the amount of energy required to initiate the process need not be as high as conventional sintering. Therefore, sintering at lower temperatures will result in final products with similar homogeneity to conventional sintering with less input energy required.
- To determine diffusion tendencies during sintering of powders, diffusion in 3D was investigated. Experiments with a copper and nickel powder blend were performed. The powder blend contained 5 wt% Cu and the remaining part was nickel. Spherical particles were chosen in order to appropriately assess diffusion in all directions. Experiments were performed at temperatures within the range of typical sintering for 30 min to ensure noticeable diffusion. It was found that diffusion in SPS is independent of orientation. Therefore, sintering at temperatures on the lower end of standard practices allows for uniform diffusion and the electric field is not a perturbing factor.
- This study showed that homogeneous distribution of elements can be obtained in SPS as long as the appropriate sintering temperature is chosen. However, the time required to reach homogeneous distribution of alloying elements is unreasonable and surpasses conventional techniques.

7 Bibliography

[1] Randall M. German. *Powder Metallurgy and Particulate Materials Processing*. Metal Powder Industries Federation, Princeton, New Jersey, 2005.

[2] R. Aalund. Spark plasma sintering. *Ceramic Industry*, 2008.

[3] Z.A. Munir, U. Anselmi-Tamburini, and M. Ohyanagi. The effect of electric field and pressure on the synthesis and consolidation of materials: A review of the spark plasma sintering method. *Journal of Materials Science*, 41:763–777, 2006.

[4] D.A. Porter and K.E. Eaterling. *Phase Transformations in Metals and Alloys*. Chapman & Hall, 2nd edition, 1981.

[5] E.A. Brandes and G.B. Brook. *Smithells Metals Reference Book (7th Edition)*. Elsevier, 1998.

[6] William D. Callister. *Material Science and Engineering An Introduction*. Jogn Wiley & Sons, Inc., 5th edition, 2000.

[7] G. Neumann and V. Tölle. Monovacancy and divancy contributions to the impurity diffusion in face-centred cubic metals. *Philosophical Magazine A*, 57(4):621–630, 1988.

[8] C. Matano. On the relation between diffusion-coefficients and concentrations of solid metals. *Japanese Journal of Physics*, 8, 1933.

[9] F. Sauer and V. Freise. Diffusion in binären gemischen mit volumenänderung. *Zeitschrift für Elektrochemie, Berichte der Bunsengesellschaft für physikalische Chemie*, 66(4):353–362, 1962.

[10] M. E. Glicksman. *Diffusion in Solids: Field Theory, Solid-State Principles, and Applications*. Number v. 1 in A Wiley-Interscience publication. Wiley, 2000.

[11] Ludwig Boltzmann. Zur integration der diffusionsgleichung bei variabeln diffusionscoefficienten. *Annalen der Physik*, 289(13):959–964, 1894.

[12] H.J. Frost and F. Ashby. *Deformation-mechanism maps: the plasticity and creep of metals and ceramics*. Pergamon Press, 1982.

[13] E.W. Hart. On the role of dislocations in bulk diffusion. *Acta Metallurgica*, 5(10):597 –, 1957.

[14] M. Tokita. Mechanism of spark plasma sintering. *Proc. of the Inter. Sympo. on Microwave, Plasma and Thermochemical Processing of Advanced Materials, S. Miyake and M. Samandi ed., Osaka Japan, JWRI Osaka University*, pages 69–76, 1997.

[15] A.V. Ragulya. Fundamentals of spark plasma sintering. In *Encyclopedia of Materials: Science and Technology (Second Edition)*, pages 1 – 5. Elsevier, Oxford, second edition edition, 2010.

[16] Nouari Saheb, Zafar Iqbal, Abdullah Khalil, Abbas Saeed Hakeem, Nasser Al Aqeeli, Tahar Laoui, Amro Al-Qutub, and René Kirchner. Spark plasma sintering of metals and metal matrix nanocomposites: a review. *Journal of Nanomaterials*, 2012:18, 2012.

[17] S.W. Wang, L.D. Chen, T. Hirai, and Y.S. Kang. Microstructure inhomogeneity in Al_2O_3 sintered bodies formed during the plasma-activated sintering process. *Journal of Materials Science Letters*, 18:1119–1121, 1999.

[18] Hisakazu Tomino, Hiroshi Watanabe, and Yoshihito Kondo. Electric current path and temperature distribution for spark sintering. *Journal of the Japan Society of Powder and Powder Metallurgy*, 44(10):974–979, 1997.

[19] Dustin M. Hulbert, André Anders, Dina V. Dudina, Joakim Andersson, Dongtao Jiang, Cosan Unuvar, Umberto Anselmi-Tamburini, Enrique J. Lavernia, and Amiya K. Mukherjee. The absence of plasma in “spark plasma sintering”. *Journal of Applied Physics*, 104(3):–, 2008.

[20] Dustin M. Hulbert, André Anders, Joakim Andersson, Enrique J. Lavernia, and Amiya K. Mukherjee. A discussion on the absence of plasma in spark plasma sintering. *Scripta Materialia*, 60(10):835 – 838, 2009.

[21] S.-X. Song, Z. Wang, and G.-P. Shi. Heating mechanism of spark plasma sintering. *Ceramics International*, 39(2):1393–1396, 2013. cited By (since 1996) 0.

[22] Subhash H. Risbud, Joanna R. Groza, and Moon J. Kim. Clean grain boundaries in aluminium nitride ceramics densified without additives by a plasma-activated sintering process. *Philosophical Magazine Part B*, 69(3):525–533, 1994.

[23] Kim Vanmeensel, Alexander Laptev, J Hennicke, Jozef Vleugels, and Omer Van der Biest. Modelling of the temperature distribution during field assisted sintering. *Acta Materialia*, 53(16):4379–4388, 2005.

[24] Antonios Zavaliangos, Jing Zhang, Martin Krammer, and Joanna R Groza. Temperature evolution during field activated sintering. *Materials Science and Engineering: A*, 379(1–2):218 – 228, 2004.

[25] Wang Yucheng and Fu Zhengyi. Study of temperature field in spark plasma sintering. *Materials Science and Engineering: B*, 90(1–2):34 – 37, 2002.

[26] G Molénat, L Durand, J Galy, and A Couret. Temperature control in spark plasma sintering: an FEM approach. *Journal of Metallurgy*, 2010, 2010.

[27] Dennis LUNDSTRÖM, Birger KARLSSON, and Mattias GUSTAVSSON. Anisotropy in thermal transport properties of cast γ-tial alloys. *Zeitschrift für Metallkunde*, 92(11):1203–1212, 2001.

[28] Salvatore Grasso, Yoshio Sakka, and Giovanni Maizza. Pressure effects on temperature distribution during spark plasma sintering with graphite sample. *Materials transactions*, 50(8):2111–2114, 2009.

[29] E.A. Olevsky and L. Froyen. Impact of thermal diffusion on densification during SPS. *Journal of the American Ceramic Society*, 92(SUPPL. 1):S122–S132, 2009. cited By (since 1996) 39.

[30] V.S. Gostomel'skii and L.V. Krupnova. Growth and healing of pores in metal under the effect of electric current pulses. *Physics and chemistry of materials treatment*, 19(4):307–310, 1985. cited By (since 1996)0.

[31] E. Olevsky and L. Froyen. Constitutive modeling of spark-plasma sintering of conductive materials. *Scripta Materialia*, 55(12):1175–1178, 2006. cited By (since 1996) 50.

[32] Lihao Ge, Ghatu Subhash, Ronald H. Baney, James S. Tulenko, and Edward McKenna. Densification of uranium dioxide fuel pellets prepared by spark plasma sintering (SPS). *Journal of Nuclear Materials*, 435:1 – 9, 2013.

[33] Jyunichi Kuchino, Kazuya Kurokawa, Tamaki Shibayama, and Heishichiro Takahashi. Effect of microstructure on oxidation resistance of $MoSi_2$ fabricated by spark plasma sintering. *Vacuum*, 73(3–4):623 – 628, 2004. The 4th International Symposium on Applied Plasma Science.

[34] Mamoru Omori. Sintering, consolidation, reaction and crystal growth by the spark plasma system (SPS). *Materials Science and Engineering: A*, 287(2):183 – 188, 2000.

[35] M Yue, J.X Zhang, W.Q Liu, and G.P Wang. Chemical stability and microstructure of Nd-Fe-B magnet prepared by spark plasma sintering. *Journal of Magnetism and Magnetic Materials*, 271(2–3):364 – 368, 2004.

[36] Z.H. Zhang, F.C. Wang, S.K. Lee, Y. Liu, J.W. Cheng, and Y. Liang. Microstructure characteristic, mechanical properties and sintering mechanism of nanocrystalline copper obtained by $\{$SPS$\}$ process. *Materials Science and Engineering: A*, 523(1–2):134 – 138, 2009.

[37] K. Ozaki, K. Kobayashi, T. Nishio, A. Matsumoto, and A. Sugiyama. Sintering phenomena on initial stage in pulsed current sintering. *Funtai Oyobi Fummatsu Yakin/Journal of the Japan Society of Powder and Powder Metallurgy*, 47(3):293–297, 2000. cited By (since 1996)27.

[38] Kazuhiro Matsugi, Tomei Hatayama, and Osamu Yanagisawa. Effect of direct current pulse discharge on specific resistivity of copper and iron powder compacts. *Nippon Kinzoku Gakkaishi/Journal of the Japan Institute of Metals*, 59(7):740–745, 1995. cited By (since 1996)57.

[39] Guoqiang Xie, Osamu Ohashi, Kentarou Chiba, Norio Yamaguchi, Minghui Song, Kazuo Furuya, and Tetsuji Noda. Frequency effect on pulse electric current sintering process of pure aluminum powder. *Materials Science and Engineering: A*, 359(1–2):384 – 390, 2003.

[40] K. Nishimoto, K. Saida, and R. Tsuduki. Effect of pulsed electric-current on densification behavior of bonded interlayer of oxide-dispersion-strengthened superalloys joint. *Nippon Kinzoku Gakkaishi/Journal of the Japan Institute of Metals*, 65(8):747–755, 2001. cited By (since 1996)22.

[41] S. Diouf and A. Molinari. Densification mechanisms in spark plasma sintering: Effect of particle size and pressure. *Powder Technology*, 221:220–227, 2012. cited By (since 1996) 2.

[42] M. Braunovic and N. Alexandrov. Intermetallic compounds at aluminum-to-copper electrical interfaces: effect of temperature and electric current. *Components, Packaging, and Manufacturing Technology, Part A, IEEE Transactions on*, 17(1):78–85, Mar 1994.

[43] J.R. Black. Electromigration—a brief survey and some recent results. *Electron Devices, IEEE Transactions on*, 16(4):338–347, 1969.

[44] E.M. Purcell and D.J. Morin. *Electricity and Magnetism*. Electricity and Magnetism. Cambridge University Press, 2013.

[45] Jason Milligan. *Surface Modification of Heat Treatable Al Components Using Cryomilled and Rapidly Solidified Al-Si*. PhD thesis, McGill University, 2013.

[46] IA Blech and Conyers Herring. Stress generation by electromigration. *Applied Physics Letters*, 29(3):131–133, 1976.

[47] I.A. Blech. Diffusional back flows during electromigration. *Acta Materialia*, 46(11):3717 – 3723, 1998.

[48] Minghui Lin and Cemal Basaran. Electromigration induced stress analysis using fully coupled mechanical–diffusion equations with nonlinear material properties. *Computational Materials Science*, 34(1):82–98, 2005.

[49] I. A. Blech. Electromigration in thin aluminum films on titanium nitride. *Journal of Applied Physics*, 47(4), 1976.

[50] W. Wu and J.S. Yuan. Copper electromigration modeling including barrier layer effect. *Solid-State Electronics*, 45(12):2011 – 2016, 2001.

[51] Wei Yao and Cemal Basaran. Electromigration damage mechanics of lead-free solder joints under pulsed DC: A computational model. *Computational Materials Science*, 71(0):76 – 88, 2013.

[52] C. Witt, C.A. Volkert, and E. Arzt. Electromigration-induced Cu motion and precipitation in bamboo Al–Cu interconnects. *Acta Materialia*, 51(1):49 – 60, 2003.

[53] L Arnaud, G Reimbold, and P Waltz. Influence of pulsed DC current stress on electromigration results in AlCu interconnections; analysis of thermal and healing effects. *Microelectronics Reliability*, 39(6):773–784, 1999.

[54] Meng Keong Lim, Jingyuan Lin, Yong Chiang Ee, Chee Mang Ng, Jun Wei, and Chee Lip Gan. Experimental characterization and modelling of electromigration lifetime under unipolar pulsed current stress. *Microelectronics Reliability*, 52(8):1553 – 1558, 2012. {ICMAT} 2011 - Reliability and variability of semiconductor devices and {ICs}.

[55] ASM International, ASM International Alloy Phase Diagram Committee, and ASM International. Handbook Committee. *ASM Handbook Volume 3: Alloy Phase Diagrams*. ASM International, 10th edition, 1992.

[56] Thermodynamic database of the phase diagrams in copper base alloy systems. *Journal of Physics and Chemistry of Solids*, 66(2–4):256 – 260, 2005. Proceedings of the 11th International Conference on High Temperature Materials Chemistry (HTMC-XI).

[57] B. Mozer, D. T. Keating, and S. C. Moss. Neutron measurement of clustering in the alloy CuNi. *Phys. Rev.*, 175:868–876, Nov 1968.

[58] J. Vrijen and S. Radelaar. Clustering in Cu-Ni alloys: A diffuse neutron-scattering study. *Phys. Rev. B*, 17:409–421, Jan 1978.

[59] M.A. Turchanin, P.G. Agraval, and A.R. Abdulov. Phase equilibria and thermodynamics of binary copper systems with 3d-metals. vi. copper-nickel system. *Powder Metallurgy and Metal Ceramics*, 46(9-10):467–477, 2007.

[60] BC Johnson, CL Bauer, and AG Jordan. Mechanisms of interdiffusion in copper/nickel thin-film couples. *Journal of applied physics*, 59(4):1147–1155, 1986.

[61] M.A. Krishtal, L.M. Shcherbakov, A.P. Mokrov, and N.A. Markova. *Fiz Metal Metalloved*, 29, 1970.

[62] S.M. Schwarz, B.W. Kempshall, and L.A. Giannuzzi. Effects of diffusion induced recrystallization on volume diffusion in the copper-nickel system. *Acta Materialia*, 51(10):2765 – 2776, 2003.

[63] P. Pichler. *Intrinsic Point Defects, Impurities, and Their Diffusion in Silicon*. Computational Microelectronics. Springer, 2004.

[64] Osamu Taguchi, Yoshiaki Iijima, and Ken ichi Hirano. Application of atomic absorption analysis to impurity diffusion of copper in nickel in a wide range of temperature. *Journal of the Japan Institute of Metals*, 48(1):20–24, 1984.

[65] C. A. Mackliet. Diffusion of iron, cobalt, and nickel in single crystals of pure copper. *Phys. Rev.*, 109:1964–1970, Mar 1958.

[66] K Monma, H Suto, and H Oikawa. Diffusion of Ni^{63} and Cu^{64} in nickel-copper alloys (on the relation between high-temperature creep and diffusion in nickel base solid solutions. II). *J. Japan Inst. Metals*, 28, 1964.

[67] K.J. Anusavice and R.T. DeHoff. Diffusion of the tracers Cu^{67}, Ni^{66}, and Zn^{65} in copper-rich solid solutions in the system Cu-Ni-Zn. *Metallurgical Transactions*, 3(5):1279–1298, 1972.

[68] T Heumann and K. J. Grundhoff. Diffusion and kirkendall effect in copper-nickel alloys. *Z. Metallkd.*, 63, 1972.

[69] G Brunel, G Cizeron, and P Lacombe. Étude de la diffusion chimique par les methodes de matano et hall dans les couples cuivre-nickel entre 800 et 1060^{o}C; variation de l'énergie d'activation en fonction de la concentration. *C.R. Acad. Sci. Paris*, C269, 1969.

[70] Daniel B. Butrymowicz, John R. Manning, and Michael E. Read. Diffusion in copper and copper alloys part iv. diffusion in systems involving elements of group viii. *Journal of Physical and Chemical Reference Data*, 5(1), 1976.

[71] Paula Horny, Eric Lifshin, Helen Campbell, and Raynald Gauvin. Development of a new quantitative x-ray microanalysis method for electron microscopy. *Microscopy and Microanalysis*, 16:821–830, 11 2010.

[72] S Paris, E Gaffet, F Bernard, and Z.A Munir. Spark plasma synthesis from mechanically activated powders: a versatile route for producing dense nanostructured iron aluminides. *Scripta Materialia*, 50(5):691 – 696, 2004.

[73] C. Rodríguez, F.J. Belzunce, C. Betegón, L. Goyos, L.A. Díaz, and R. Torrecillas. Nanostructured Al–$ZrAl_3$ materials consolidated via spark plasma sintering: Evaluation of their mechanical properties. *Journal of Alloys and Compounds*, 550(0):402 – 405, 2013.

[74] Xiaoqiang Li, Ke Hu, Shengguan Qu, Li Li, and Chao Yang. 93w–5.6ni–1.4fe heavy alloys with enhanced performance prepared by cyclic spark plasma sintering. *Materials Science and Engineering: A*, 599(0):233 – 241, 2014.

[75] Teresa Hungria, Jean Galy, and Alicia Castro. Spark plasma sintering as a useful technique to the nanostructuration of piezo-ferroelectric materials. *Advanced Engineering Materials*, 11(8):615–631, 2009.

[76] J. Zhao, J.E. Garay, U. Anselmi-Tamburini, and Z.A. Munir. Directional electromigration-enhanced interdiffususion in the Cu-Ni system. *Journal of Applied Physics*, 102(11), 2007.

[77] Jing Jiang, Seongtae Bae, and Sunwook Kim. Effects of Cu interdiffusion on the electromigration failure of FM/Cu/FM tri-layers for spin valve read sensors. *Magnetics, IEEE Transactions on*, 43(6):2836–2838, June 2007.

[78] A.R. Grone. Current-induced marker motion in copper. *Journal of Physics and Chemistry of Solids*, 20(1–2):88 – 93, 1961.

[79] G. O. Tronsdal and H. Sorum. Interdiffusion in Cu-Ni, Co-Ni, and Co-Cu. *physica status solidi (b)*, 4(3):493–498, 1964.

[80] R.A. Matula, Center for Information, Numerical Data Analysis, and Purdue University Synthesis. *Electrical Resistivity of Copper, Gold, Palladium, and Silver*. American Chemical Society, 1979.

[81] N.F. Mott. Electrons in transition metals. *Advances in Physics*, 13(51):325–422, 1964.

[82] J. Callaway and C. S. Wang. Self-consistent calculation of energy bands in ferromagnetic nickel. *Phys. Rev. B*, 7:1096–1103, Feb 1973.

[83] S.N. Piramanayagam and T.C. Chong. *Developments in Data Storage: Materials Perspective*. Wiley, 2011.

[84] R. N. Sinclair and B. N. Brockhouse. Dispersion relation for spin waves in a FCC cobalt alloy. *Phys. Rev.*, 120:1638–1640, Dec 1960.

[85] R. D. Lowde. Spin fluctuation scattering of neutrons and the ferromagnetic state in iron. *Proceedings of the Royal Society of London. Series A, Mathematical and Physical Sciences*, 235(1202):305–320, 1956.

[86] P.E. Tannenwald and R. Weber. Exchange integral in cobalt from spin-wave resonance. *Physical Review*, 121(3):715, 1961. cited By (since 1996)29.

[87] D.D. Stancil and A. Prabhakar. *Spin Waves: Theory and Applications*. Springer, 2009.

[88] N.F. Mott and H. Jones. *The Theory of the Properties of Metals and Alloys*. Dover books on physics and mathematical physics. Dover Publications, 1958.

[89] A. Nilsson, L.G.M. Pettersson, and J. Norskov. *Chemical Bonding at Surfaces and Interfaces*. Elsevier Science, 2011.

[90] J. Friedel. Electronic structure of primary solid solutions in metals. *Advances in Physics*, 3(12):446–507, 1954.

[91] J. Friedel. On some electrical and magnetic properties of metallic solid solutions. *Canadian Journal of Physics*, 34(12A):1190–1211, 1956.

[92] de Faget de Casteljau, P. and Friedel, J. Étude de la résistivité et du pouvoir thermoélectrique des impuretés dissoutes dans les métaux nobles. *J. Phys. Radium*, 17(1):27–32, 1956.

[93] D. R. Salahub and F. Raatz. Effects of chemisorption and alloying on the magnetism of nickel clusters. *International Journal of Quantum Chemistry*, 26(S18):173–182, 1984.

[94] R Poerschke, U Theis, and H Wollenberger. Equilibrium and kinetics of the short-range atomic clustering in nickel-copper alloys. *Journal of Physics F: Metal Physics*, 10(1):67, 1980.

[95] S. Chikazumi and C.D. Graham. *Physics of Ferromagnetism 2e*. International Series of Monographs on Physics. OUP Oxford, 2009.

[96] G. Bertrand, M. Lallemant, and G. Watelle. Propos sur l'interpretation de l'énergie d'activation experimentale. *Journal of thermal analysis*, 13(3):525–542, 1978.

[97] Yu Sun, Kaustubh Kulkarni, AnilK. Sachdev, and EnriqueJ. Lavernia. Synthesis of γ-TiAl by reactive spark plasma sintering of cryomilled Ti and Al powder blend, part I: Influence of processing and microstructural evolution. *Metallurgical and Materials Transactions A*, 45(6):2750–2758, 2014.

[98] T Murakami, A Kitahara, Y Koga, M Kawahara, H Inui, and M Yamaguchi. Microstructure of Nb–Al powders consolidated by spark plasma sintering process. *Materials Science and Engineering: A*, 239–240(0):672 – 679, 1997. 4th Conference on High-Temperature Intermetallics.

[99] G.L. Burenkov, A.I. Raichenko, and A.M. Suraeva. Macroscopic mechanism of formation of interparticle contact in electric current sintering of powders. *Soviet Powder Metallurgy and Metal Ceramics*, 28(3):186–191, 1989.

[100] M.Z. Kol'chinskii and A.I. Raichenko. A model investigation of the sintering of metal powders with intense energy release at inter-particle contacts. *Soviet Powder Metallurgy and Metal Ceramics*, 16(8):585–588, 1977.